

Functional subdivisions of medial parieto-occipital cortex in humans and nonhuman primates using resting-state fMRI



R. Matthew Hutchison^{a,b,c,*}, Jody C. Culham^{d,e}, J. Randall Flanagan^{f,g}, Stefan Everling^{c,d}, Jason P. Gallivan^{f,g,**}

^a Department of Psychology, Harvard University, Cambridge, MA, USA

^b Center for Brain Science, Harvard University, Cambridge, MA, USA

^c Robarts Research Institute, University of Western Ontario, London, Ontario, Canada

^d Brain and Mind Institute, University of Western Ontario, London, Ontario, Canada

^e Department of Psychology, University of Western Ontario, London, Ontario, Canada

^f Centre for Neuroscience Studies, Queen's University, Kingston, Ontario, Canada

^g Department of Psychology, Queen's University, Kingston, Ontario, Canada

ARTICLE INFO

Article history:

Received 7 February 2015

Accepted 29 April 2015

Available online 10 May 2015

Keywords:

Functional connectivity

Homologies

Macaque

Parietal cortex

mPOC

ABSTRACT

Based on its diverse and wide-spread patterns of connectivity, primate posteromedial cortex (PMC) is well positioned to support roles in several aspects of sensory-, cognitive- and motor-related processing. Previous work in both humans and non-human primates (NHPs) using resting-state functional MRI (rs-fMRI) suggests that a subregion of PMC, the medial parieto-occipital cortex (mPOC), by virtue of its intrinsic functional connectivity (FC) with visual cortex, may only play a role in higher-order visual processing. Recent neuroanatomical tracer studies in NHPs, however, demonstrate that mPOC also has prominent cortico-cortical connections with several frontoparietal structures involved in movement planning and control, a finding consistent with increasing observations of reach- and grasp-related activity in the mPOC of both NHPs and humans. To reconcile these observations, here we used rs-fMRI data collected from both awake humans and anesthetized macaque monkeys to more closely examine and compare parcellations of mPOC across species and explore the FC patterns associated with these subdivisions. Seed-based and voxel-wise hierarchical cluster analyses revealed four broad spatially separated functional boundaries that correspond with graded differences in whole-brain FC patterns in each species. The patterns of FC observed are consistent with mPOC forming a critical hub of networks involved in action planning and control, spatial navigation, and working memory. In addition, our comparison between species indicates that while there are several similarities, there may be some species-specific differences in functional neural organization. These findings and the associated theoretical implications are discussed.

© 2015 Elsevier Inc. All rights reserved.

Introduction

The posteromedial cortex (PMC), comprising the precuneus, retrosplenial, and posterior cingulate cortex, is a highly diverse anatomical structure implicated in vast array of higher order cognitive functions and behaviors. In humans, specific sets of cognitive functions have been ascribed to particular subregions of PMC. For example, neural activation responses in dorsal-anterior PMC have been linked to self-referential processes like mental imagery, covert shifts of attention (Cavanna and Trimble, 2006), and the preparation and execution of visually guided behaviors (Wenderoth et al., 2005). Responses associated with

dorsal-posterior PMC have been linked to episodic memory retrieval and the processing of emotions (Lundstrom et al., 2003; Lundstrom et al., 2005; Cavanna and Trimble, 2006; Dorfel et al., 2009). In addition, ventral PMC, and the posterior cingulate cortex (PCC) in particular, has been identified as a key hub of the default network (DN), an interconnected set of cortical areas that include the inferior parietal lobule, hippocampal formation, and superior frontal and medial frontal gyri. The DN has been functionally implicated in internal modes of cognition such as autobiographical memory retrieval and envisioning the future (for review, see Buckner et al., 2008), as well as elements of consciousness (Maquet et al., 1997; Fiset et al., 1999; Canavero et al., 2009) and social cognition (Schilbach et al., 2008; Schilbach et al., 2012). Taken together, the available functional evidence implicates the PMC as being heterogeneous and playing an associative and/or integrative role in several aspects of higher-level cognitive processing.

The vast array of cognitive functions ascribed to the PMC matches well with the host of cytoarchitectonic divisions of which it is comprised. Though Brodmann (1909, 2006) originally parcellated the

* Correspondence to: R.M. Hutchison, Center for Brain Science, Harvard University, Cambridge, MA, USA.

** Correspondence to: J.P. Gallivan, Department of Psychology, Centre for Neuroscience Studies, Queen's University, Kingston, Ontario K7L 3N6, Canada.

E-mail addresses: rhutchison@FAS.Harvard.edu (R.M. Hutchison), jasongallivan@gmail.com (J.P. Gallivan).

PMC into five subregions (areas 23, 29, 30, 31, and 7; see Fig. 1), other anatomists of the 20th century—and even Brodmann himself—have suggested that more cytoarchitectonic subdivisions may exist, particularly within the precuneus (Smith, 1907; Vogt, 1911; Economo and Koskinas, 1925; Von Bonin and Bailey, 1947; Pandya and Seltzer, 1982; Cavada and Goldman-Raiuc, 1989; Scheperjans et al., 2008b; Scheperjans et al., 2008a). Axonal tract tracing studies in monkeys suggest a posterior-to-anterior transitional gradient in the precuneus on the basis of cortico-cortical connectivity patterns, with three broader subdivisions emerging: posterior (area PO), middle (area PGm), and anterior (area PEc). On the basis of its prominent connections to occipital cortex, area PO, which spans the dorsal parieto-occipital sulcus (POS) in mPOC, was thought to primarily play a role in visual processing (Colby et al., 1988). However, more recent evidence from the field of sensorimotor neuroscience has demonstrated functional neuronal properties and patterns of cortico-cortical connectivity in the macaque monkey that are also consistent with the area and its immediate surrounding cortex playing an important role in visuomotor planning and control. In particular, converging work indicates that area PO, and mPOC more generally, rather than being a single homogeneous structure, is actually comprised of three distinct areas, V6, V6Av, and V6Ad (Galletti et al., 2005). These regions differ in their topography, cytoarchitectonics, and structural connections (Galletti et al., 2001; Gamberini et al., 2009; Passarelli et al., 2011), and area V6A has

neuronal responses that correspond with visuomotor transformations required for manual behaviors like reaching and grasping (Fattori et al., 2009b; Fattori et al., 2010; Gamberini et al., 2011; Fattori et al., 2012).

In support of functional homologies between the mPOC region of macaques and humans, recent studies using wide-field retinotopic mapping have identified putative human homologues of monkey areas V6 (Pitzalis et al., 2006; Fattori et al., 2009a; Pitzalis et al., 2010) and V6Av (Pitzalis et al., 2013a). Moreover, convergent findings from fMRI (e.g., Prado et al., 2005; Gallivan et al., 2011a; Gallivan et al., 2011b; Tosoni et al., 2014), transcranial magnetic stimulation (e.g., Vesia et al., 2010; Ciavarro et al., 2013), and patient studies (Karnath and Perenin, 2005) all implicate the region surrounding the superior aspect of the POS, the superior parieto-occipital cortex (SPOC), in the preparation and execution of reaching and grasping actions. Despite considerable differences in the methodologies employed in the two species, both macaque and human mPOC appear to have a similar functional neural organization.

Resting-state functional MRI (rs-fMRI) approaches, which typically exploit temporal dependencies of low-frequency blood oxygenation level-dependent (BOLD) oscillations to reveal functional networks in the absence of any explicit task paradigm (Biswal et al., 1995), have emerged as a simple yet powerful tool for comparing the functional neural organization of the human and nonhuman primate (NHP) brains (Vincent et al., 2007; Margulies et al., 2009; Hutchison et al., 2011; Mars

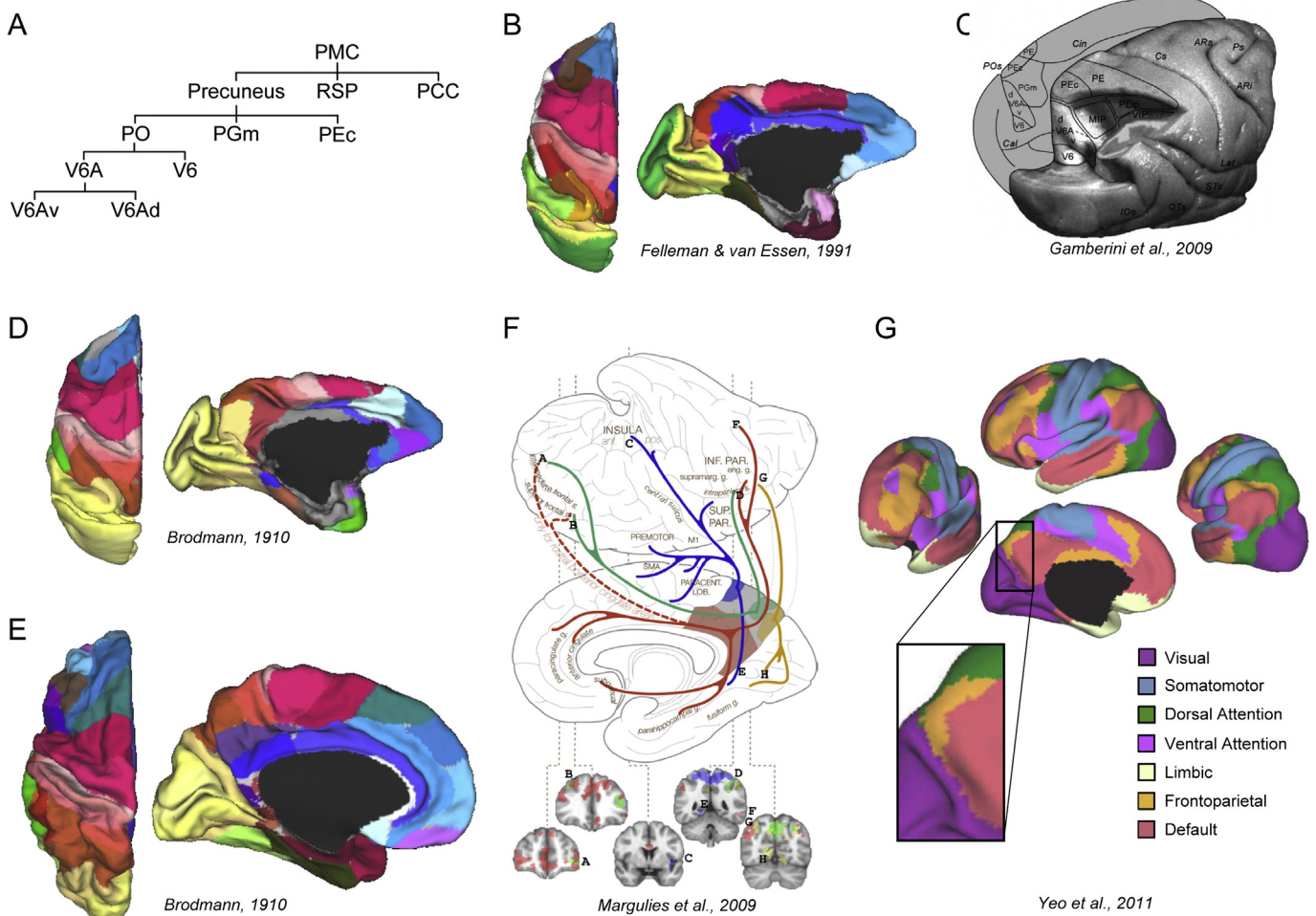


Fig. 1. Previous parcellations of mPOC based on cytoarchitectonics, cortico-cortical connections and functional neural response properties. A) Nomenclature of proposed subdivisions of macaque posteromedial cortex (PMC). RSP = retrosplenial cortex; PCC = posterior cingulate cortex. B–D) Proposed parcellations in the macaque. B) Cytoarchitectonic divisions proposed by Felleman & van Essen. C) Subdivisions, based on cytoarchitectonics, cortico-cortical connections and neurophysiological recordings, proposed by Galletti, Fattori and colleagues. D) Cytoarchitectonic divisions proposed by Brodmann. E–G) Proposed parcellations in the human. E) Cytoarchitectonic divisions proposed by Brodmann. F) Functional subdivisions, based on intrinsic patterns of functional connectivity, proposed by Margulies et al. (2009). G) Whole-brain network parcellations, based on intrinsic patterns of functional connectivity, proposed by Yeo et al. (2011). Inset shows close-up of mPOC parcellation, with colors denoting proposed functional subdivisions for a 7 cluster network.

et al., 2011; Hutchison and Everling, 2012; Hutchison et al., 2012c; Hutchison et al., 2012a; Sallet et al., 2013; Neubert et al., 2014). Its usefulness stems from the fact that it circumvents the practical limitations of having to employ invasive methodologies in the human (i.e., electrophysiological recordings) while, at the same time, avoiding the necessity of long behavioral training regimens so that macaques are able to perform complex behavioral tasks while in the MRI scanner environment. While some previous work has already provided rs-fMRI parcellations of human PMC (Cauda et al., 2010; Zhang and Li, 2012; Zhang et al., 2014) there exists only one previous study that explored the functional correspondence between macaque and human PMC (Margulies et al., 2009). The seed-based rs-fMRI parcellation by Margulies and colleagues differentiated the right PMC into five regions, three of which were in the precuneus, subdivided posteriorly-to-anteriorly, with the remaining two regions being in the posterior cingulate, subdivided rostral-caudally. Notably, these authors only reported sensorimotor-like network activity associated with their anterior-most dorsal seed cluster in both species, a finding consistent with some of the connectivity patterns of the anterior portion of the precuneus (PEc) in macaques (Morecraft et al., 2004) and previous reports of movement-related activity in the anterior precuneus of humans (Wenderoth et al., 2005). However, this sensorimotor pattern of FC being unique to anterior precuneus contrasts with much more recent anatomical delineations of macaque mPOC (i.e., based on cytoarchitectonics and cortico-cortical connectivity patterns, see Gamberini et al., 2009; Bakola et al., 2010; Passarelli et al., 2011) and convergent findings of reach- and grasp-related activations in the SPOC of both species (Fattori et al., 2009b; Fattori et al., 2010; Fattori et al., 2012), as noted above. Further comparative rs-fMRI work could help reconcile this emerging sensorimotor role being attributed to mPOC in both the macaque and human.

In light of mounting evidence supporting a visual–motor function for SPOC, the goal of the present study was to, rather than examining the PMC as a whole or some of its subsections individually (as done previously, see Margulies et al., 2009; Leech et al., 2012), provide a more systematic and detailed investigation of the FC of the cortex directly adjacent to the POS and examine the degree of correspondence between the two primate species. We hypothesized that by focusing our investigation on the precuneus in particular, we might reveal more nuanced patterns of FC much more in line with the cortico-cortical connectivity patterns and sensorimotor profiles of neural responses observed in recent macaque and human work on the area.

Materials and methods

Overview

Resting-state fMRI data was collected from anesthetized macaques ($N = 11$) and awake humans ($N = 23$). Thirty-six spherical seed regions were placed in each species anteriorly and posteriorly to the POS based on anatomical landmarks. Using the extracted timecourses from these regions, hierarchical clustering and whole-brain, voxel-wise functional connectivity analysis was performed.

Additionally, voxel-wise clustering of voxels within the mPOC was performed based on local temporal relationships within the mPOC and whole-brain connectivity fingerprints.

Monkey

Participants

Data was collected from eleven naïve, isoflurane-anesthetized (1%) macaque monkeys (4 *Macaca mulatta*, 7 *Macaca fascicularis*; 4 female). All surgical and experimental procedures were carried out in accordance with the Canadian Council of Animal Care policy on the use of laboratory animals and approved by the Animal Use Subcommittee of the University of Western Ontario Council on Animal Care. Portions

of these data have been previously published together (Hutchison and Everling, 2013) and within two different datasets: Set 1 (TR = 2 s, EPI resolution = 1.3 mm × 1.3 mm × 1.5 mm, 2 scans of 300 volumes; (Hutchison et al., 2011)) and Set 2 (TR = 2 s, EPI resolution = 1 mm × 1 mm × 1 mm, 10 scans of 150 volumes; (Babapoor-Farrokhran et al., 2013)). One monkey from Set 1 was scanned again with the increased spatial resolution and scan numbers of Set 2, and so the original scanning session from Set 1 was removed from the analysis, leaving a total of 11 naïve animals.

Preparation

All animals were previously implanted with an MRI-compatible custom-built acrylic head post that was anchored to the skull with 6-mm ceramic bone screws (Thomas Recording, Giessen, Germany) and dental acrylic to allow restraint of the head during data collection. Anesthesia was utilized in this study to eliminate motion effects, physiological stress, and training requirements. In preparation for image acquisition, monkeys were injected intramuscularly with atropine (0.4 mg/kg), ipratropium (0.025 mg/kg), and ketamine hydrochloride (7.5 mg/kg), followed by intravenous administration of 3 ml propofol (10 mg/ml) via the saphenous vein. Animals were then intubated and switched to 1.5% isoflurane mixed with oxygen. Each monkey was then placed in a custom-built monkey chair with its head immobilized using the head post, and inserted into the magnet bore, at which time the isoflurane level was lowered to 1.0% and allowed to stabilize as localizer and anatomical scans were acquired. Although isoflurane has been shown to have vasodilator properties (Farber et al., 1997) that can alter the neurovascular coupling (for review, see Masamoto and Kanno, 2012), synchronous spontaneous BOLD fluctuations have been reported using an isoflurane regime in both monkeys (Vincent et al., 2007) and rats (Hutchison et al., 2010). Increasing the anesthetic dosage can lead to decreased coherence of functional networks (Vincent et al., 2007; Hutchison et al., 2014a), and thus the lowest dose needed to maintain immobility was used here.

Rectal temperature via a fiber-optic temperature probe (FISO, Quebec City, QC), respiration via bellows (Siemens Corp., Union, NJ), and end-tidal CO₂ via capnometer (Covidien-Nellcor, Boulder, CO) were monitored throughout the scan. Warmth was maintained using a heating disk (Snugglesafe, Littlehampton, West Sussex, UK) and thermal insulation.

MRI acquisition

Data were acquired on an actively shielded 7-T 68-cm horizontal bore scanner with a DirectDrive console (Agilent, Santa Clara, California) with a Siemens AC84 gradient subsystem (Erlangen, Germany) operating at a slew rate of 350 mT/m/s. An in-house designed and manufactured conformal five-channel transceiver primate-head RF coil was used for all experiments. Magnetic field optimization (B₀ shimming) was performed using an automated three-dimensional mapping procedure over the specific imaging volume of interest.

In data from Set 1 ($N = 5$), 2 scans (defined here as the acquisition of time series of 3D volumes) of 300 continuous EPI functional volumes (TR = 2000 ms; TE = 16 ms; flip angle = 70°, slices = 30, matrix = 72 × 72; FOV = 96 × 96 mm; acquisition voxel size = 1.3 mm × 1.3 mm × 1.5 mm) were acquired in each animal. Acquisition time of each scan was 5 min. EPI images were acquired with GRAPPA at an acceleration factor of 2. Every image was corrected for physiological fluctuations using navigator echo correction. A high-resolution T2-weighted anatomical reference volume was acquired along the same orientation as the functional images using a fast spin echo acquisition scheme (TR = 5000 ms; TE = 38.6 ms; echo train length = 5, effective echo = 3, slices = 30, matrix = 256 × 250; FOV = 96 mm × 96 mm; acquisition voxel size = 375 μm × 384 μm × 1.5 mm).

In data from Set 2 ($N = 6$), 10 scans of 150 EPI functional volumes (TR = 2000 ms, TE = 16 ms, flip angle = 70°, matrix = 96 × 96,

FOV = 96 mm × 96 mm, acquisition voxel size = 1 mm × 1 mm × 1 mm) were acquired in each animal. Acquisition time of each scan was 5 min. EPI images were acquired with GRAPPA at an acceleration factor of 2. Every image was corrected for physiological fluctuations using navigator echo correction. A high-resolution gradient echo (GRE) anatomic MR image was acquired along the same orientation as the functional images (TR = 1100 ms, TE = 8 ms, matrix = 256 × 256, FOV = 96 × 96 mm, acquisition voxel size = 375 μm × 375 μm × 1 mm). Also, for every monkey, a T1-weighted anatomic image (TE = 2.5 ms, TR = 2300 ms, TI = 800 ms, FOV = 96 × 96 mm, acquisition voxel size = 750 μm × 750 μm × 750 μm) was acquired.

Preprocessing

Functional image preprocessing was implemented in the FMRIB Software Library toolbox (FSL; <http://www.fmrib.ox.ac.uk>). This consisted of motion correction (6-parameter affine transformation), brain extraction, spatial smoothing (Gaussian kernel of full-width at half maximum [FWHM] 3 mm applied to each volume separately), high-pass temporal filtering (Gaussian-weighted least-squares straight line fitting with sigma = 100 s), low-pass temporal filtering (half-width at half maximum = 2.8 s, Gaussian filter), and normalization (12 DOF linear affine transformation) to the F99 atlas template (Van Essen, 2004, see <http://sumsdb.wustl.edu/sums/macaquemore.do>). Global mean signal regression was not implemented for the primary analyses because of concerns of artificially introducing negative correlations into the connectivity maps (Murphy et al., 2009) and evidence that the global mean signal may in fact have an underlying neural component (Scholvinck et al., 2010). Nevertheless, to illustrate the potential effects of global mean signal regression, we repeated the analysis partialling out the mean whole-brain signal and found qualitatively similar results in both species (see Supplementary Fig. 1).

Seed selection

A total of 36 (18 per hemisphere) spherical seed ROIs (radius = 1 mm) were created in the F99 atlas space (Van Essen, 2004, Table 1; Fig. 2A left). Parallel lines of approximately equidistant seeds were placed in the gray matter using the POS as a reference. Two medial rows (seeds 1–4 and 5–8) and one lateral row (seeds 9–12) were placed anteriorly to the POS. One medial (seeds 13–15) and one lateral (seeds 16–18) row were placed posteriorly to the POS. There was no overlap of seeds in any dimension and the placement of all the seeds ensured that none of the constituent voxels extended outside the gray matter (into the white matter or into the medial longitudinal fissure). Here,

we provide the details of seed placement (for both the left and right hemispheres) in the macaque F99 brain (for F99 coordinates of each seed region, see Table 1).

Seed 1: Located directly anterior to the parieto-occipital sulcus (POS) and dorsal to its ventro-anterior arc, corresponding cytoarchitecturally to areas V6/V6A (Gamberini et al., 2009).

Seed 2: Located dorsal to Seed 1, parallel to the POS, corresponding cytoarchitecturally to area V6A.

Seed 3: Located dorsal to Seed 2, parallel to the POS, corresponding cytoarchitecturally to areas V6A/PGm.

Seed 4: Located dorsal to Seed 3, parallel to the POS, corresponding cytoarchitecturally to areas Péc/PGm.

Seed 5: Located directly anterior to Seed 1, in approximately the same x and z plane, corresponding cytoarchitecturally to areas V6/V6A.

Seed 6: Located directly anterior to Seed 2, in approximately the same x and z plane, corresponding cytoarchitecturally to area V6A.

Seed 7: Located directly anterior to Seed 3, in approximately the same x and z plane, corresponding cytoarchitecturally to area PGm.

Seed 8: Located directly anterior to Seed 4, in approximately the same x and z plane, corresponding cytoarchitecturally to areas Péc/PGm.

Seed 9: Located 2 mm lateral to Seed 1, in approximately the same y and z plane.

Seed 10: Located 2 mm lateral to Seed 2, in approximately the same y and z plane.

Seed 11: Located 2 mm lateral to Seed 3, in approximately the same y and z plane.

Seed 12: Located 2 mm lateral to Seed 4, in approximately the same y and z plane.

Seed 13: Located directly posterior to the POS, and in approximately the same x and z plane as Seed 1.

Seed 14: Located dorsal to Seed 13, parallel to the POS, and in approximately the same x and z plane as Seed 2.

Seed 15: Located dorsal to Seed 14, parallel to the POS, and in approximately the same x and z plane as Seed 3.

Seed 16: Located 2 mm lateral to Seed 13, in approximately the same y and z plane.

Seed 17: Located 2 mm lateral to Seed 14, in approximately the same y and z plane.

Seed 18: Located 2 mm lateral to Seed 15, in approximately the same y and z plane.

Humans

Participants

Previously published data (Hutchison et al., 2014b) from twenty-three right-handed volunteers (12 females; mean age = 24.8 years), recruited from the Western University (London, Ontario, Canada; N = 11) and Queen's University (Kingston, Ontario, Canada; N = 12) were used in this study. Informed consent was obtained in accordance with procedures approved by each University's Health Sciences Research Ethics Board.

MRI acquisition

Imaging was performed on 3-T Siemens TIM MAGNETOM Trio MRI scanners located at the Centre for Functional and Metabolic Mapping (CFMM; at Western University) and the Centre for Neuroscience Studies (CNS; at Queen's University). For each participant, all functional data was collected using a T2*-weighted single-shot

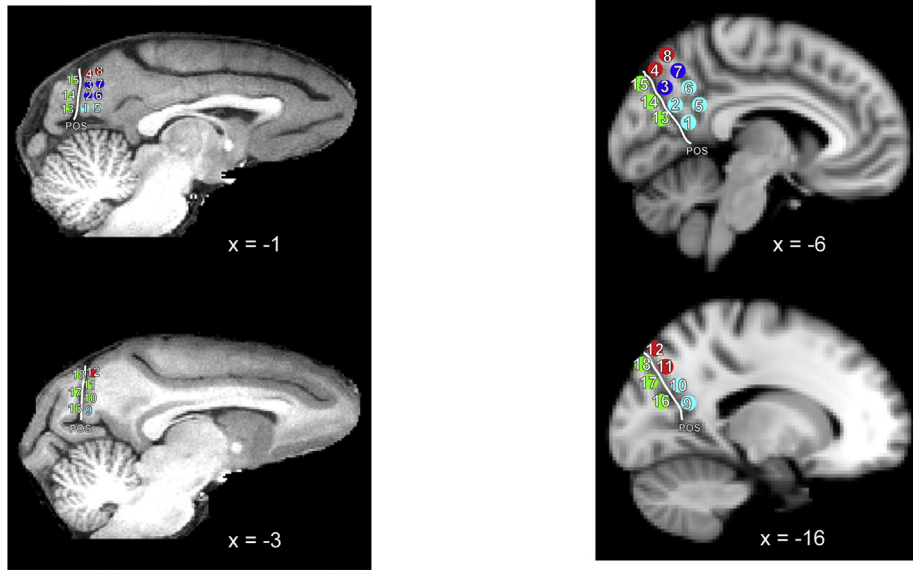
Table 1
Seed-region locations.

ROI	Monkey coordinates ^a	Human coordinates ^b
1	± 1.01/– 34.71/9.56	± 6/– 58/16
2	± 1.01/– 34.20/12.58	± 6/– 66/26
3	± 1.01/– 33.70/15.09	± 6/– 72/36
4	± 1.01/– 33.70/17.61	± 6/– 78/46
5	± 1.01/– 31.69/9.56	± 6/– 52/26
6	± 1.01/– 31.69/12.58	± 6/– 58/36
7	± 1.01/– 31.19/15.59	± 6/– 64/46
8	± 1.01/– 31.19/18.61	± 6/– 72/54
9	± 3.02/– 35.21/9.56	± 16/– 58/18
10	± 3.02/– 35.21/12.58	± 16/– 64/28
11	± 3.02/– 35.21/15.59	± 16/– 72/40
12	± 3.02/– 34.20/18.61	± 16/– 78/50
13	± 1.01/– 38.73/9.56	± 6/– 74/18
14	± 1.01/– 38.28/12.58	± 6/– 80/30
15	± 1.01/– 37.72/16.10	± 6/– 86/38
16	± 3.02/– 35.23/10.06	± 16/– 74/20
17	± 3.02/– 38.23/13.58	± 16/– 78/32
18	± 3.02/– 37.72/18.11	± 16/– 84/42

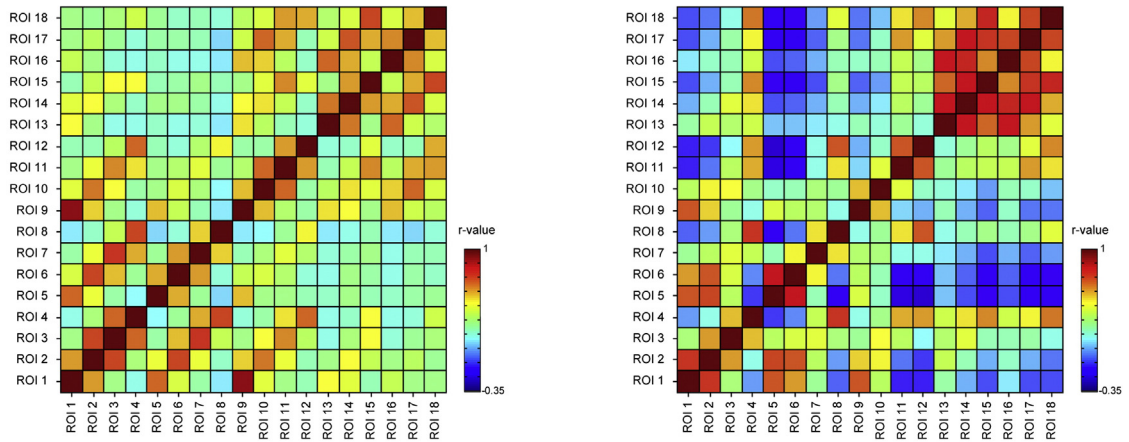
^a F99 atlas space.

^b MNI152 atlas space.

A Seed Regions



B Temporal Relationships



C Hierarchical Clustering

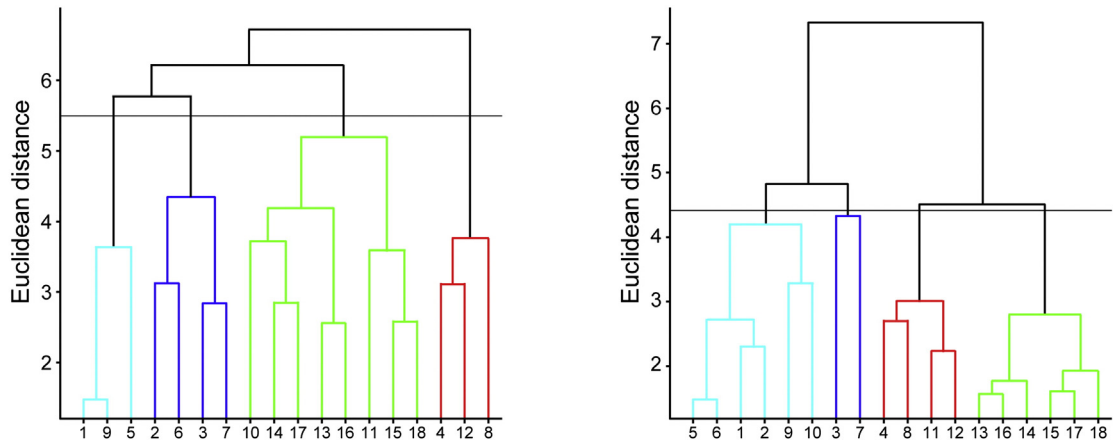


Fig. 2. Analysis of macaque and human mPOC seed ROIs. A) mPOC seed ROIs. The locations of 18 spherical seed ROIs for both the macaque monkey (left; radius = 1 mm) and human (right; radius = 4 mm), displayed to scale on midsagittal slices of the macaque F99 (left; Van Essen, 2004) and human PALS-B12 (right; Van Essen, 2005) template, respectively. Parallel rows of seeds were placed both posteriorly and anteriorly to the parieto-occipital sulcus (POS) at two different depths in the midsagittal plane (medial (top) and lateral (bottom)). Seeds were placed color-coded according to their cluster assignment following hierarchical cluster analysis (shown in C). For illustrative purposes, the sizes of the seed regions have been slightly magnified in each species. B) Average pairwise correlation matrix of resting-state BOLD time series between mPOC seed ROIs for both the macaque (left) and human (right). The color of each cell of the matrix denotes the corresponding pairwise coefficient value (according to the color bar at right). C) Dendrogram plots, for both the macaque (left) and human (right), of the hierarchical binary cluster tree of mPOC seed ROIs following cluster analysis (based on Euclidean distance of the correlation coefficients in B).

gradient-echo echo planar imaging (EPI) acquisition sequence (repetition time [TR] = 2000 ms; slice thickness = 3 mm; in-plane resolution = 3 mm × 3 mm; echo time [TE] = 30 ms; field of view [FOV] = 240 mm × 240 mm; matrix size = 80 × 80; flip angle = 90°) with 32-channel (at CFMM) or 12-channel (at CNS) receive-only head coils. Each volume was comprised of 34 contiguous (no gap) oblique slices acquired at a ~30° caudal tilt with respect to the plane of the anterior commissure and posterior commissure (AC–PC), providing near whole brain coverage. One resting-state scan of 360 continuous functional volumes was collected (acquisition time of each scan was 12 min). A T1-weighted high-resolution anatomical image was collected using an ADNI MPRAGE sequence (TR = 2300 ms; TE = 2.98 ms; FOV = 192 mm × 240 mm × 256 mm; matrix size = 192 × 240 × 256; flip angle = 9°; acquisition voxel size = 1 mm × 1 mm × 1 mm). The resting-state scans and a second anatomical image were acquired in a separate session in four participants due to time constraints imposed during the initial imaging session.

Preprocessing

Preprocessing was implemented using the FMRIB Software Library toolbox (FSL, <http://www.fmrib.ox.ac.uk>, Smith et al., 2004; Woolrich et al., 2009) and included slice time correction for interleaved acquisitions (using Fourier-space time-series phase shifting), motion correction (six parameter affine transformation), brain extraction, spatial smoothing (Gaussian kernel of full-width at half-maximum [FWHM] 6 mm applied to each volume separately), low-pass temporal filtering (half-width at half-maximum [HWHM] = 2.8 s, Gaussian filter), high-pass temporal filtering (Gaussian weighted least-squares straight line fitting with sigma = 100 s), and normalization (12 degrees-of-freedom linear affine transformation) to the standard 152-brain MNI template (voxel size = 2 mm × 2 mm × 2 mm; Evans et al., 1993). Global mean signal regression was not implemented (see Monkey preprocessing). Note that motion was relatively minimal across the human subjects. The mean relative displacement was 0.06 mm. The mean number of micro- (0.1–0.5 mm) and macro-movements (>0.5 mm) was 22.35 ± 45.09 and 0.65 ± 1.37, respectively.

Seed selection

A total of 36 (18 per hemisphere) spherical seed ROIs (radius = 4 mm) were created in the MNI atlas space (Evans et al., 1993, Table 1; Fig. 2A right). Parallel lines of approximately equidistant seeds were placed in the gray matter using the parieto-occipital sulcus (POS) as a reference. Two medial (seeds 1–4 and 5–8) rows and one lateral (seeds 9–12) row were placed anteriorly to the POS. In addition, one medial (seeds 13–15) row and one lateral (seeds 16–18) row were placed posteriorly to the POS. There was no overlap of seeds in any dimension and the placement of all the seeds ensured that none of the constituent voxels extended outside the gray matter (into white matter or into the medial longitudinal fissure). Here, we provide the details of seed placement (for both the left and right hemispheres) in the MNI152 brain (for MNI coordinates of each seed region, see Table 1).

Seed 1: Located directly anterior to the parieto-occipital sulcus (POS), positioned directly posterior to the posterior, inferior arc of the subparietal sulcus, corresponding cytoarchitecturally to Brodmann areas 30/23 (Duvernoy et al., 2012).

Seed 2: Located dorsal to Seed 1, parallel to the POS, corresponding cytoarchitecturally to areas 23/31.

Seed 3: Located dorsal to Seed 2, parallel to the POS, corresponding cytoarchitecturally to areas 31/7b.

Seed 4: Located dorsal to Seed 3, parallel to the POS, corresponding cytoarchitecturally to area 7b.

Seed 5: Located dorsal-anteriorly to Seed 4, positioned in the posterior, inferior arc of the subparietal sulcus, corresponding cytoarchitecturally to area 23.

Seed 6: Located dorsal to Seed 5 and dorso-anteriorly from Seed 2, corresponding cytoarchitecturally to areas 23/31.

Seed 7: Located dorsal to Seed 6 and dorso-anteriorly from Seed 3, corresponding cytoarchitecturally to areas 31/7b.

Seed 8: Located dorsal to Seed 7 and dorso-anteriorly from Seed 4, corresponding cytoarchitecturally to area 7b.

Seed 9: Located 10 mm lateral to Seed 1, in approximately the same y and z plane.

Seed 10: Located 10 mm lateral to Seed 2, in approximately the same y and z plane.

Seed 11: Located 10 mm lateral to Seed 3, in approximately the same y and z plane.

Seed 12: Located 10 mm lateral to Seed 4, in approximately the same y and z plane.

Seed 13: Located directly posterior to the POS, above the calcarine sulcus, and positioned postero-ventrally from Seed 2, corresponding cytoarchitecturally to areas 17/18.

Seed 14: Located dorsal to Seed 13, parallel to the POS, corresponding cytoarchitecturally to areas 18/19.

Seed 15: Located dorsal to Seed 14, parallel to the POS, corresponding cytoarchitecturally to area 19.

Seed 16: Located 10 mm lateral to Seed 13, in approximately the same y and z plane.

Seed 17: Located 10 mm lateral to Seed 14, in approximately the same y and z plane.

Seed 18: Located 10 mm lateral to Seed 15, in approximately the same y and z plane.

Analysis

SNR maps

We computed the group-average voxel-wise signal-to-noise ratio (SNR) of both species to estimate the effects of susceptibility artifacts in the present data. For each voxel of a scan, the average signal intensity across the scan was divided by the standard deviation over time. In monkeys, the voxel-wise SNR values were averaged between scans of each individual and then across animals to compute the group average. In humans, where only a single resting-state scan was collected, the final group-averaged SNR map was calculated by averaging SNR maps across all participants. The group averaged SNR maps of both species can be seen projected onto the cortical surface in Supplementary Fig. 2. While there is variation across the cortex and relatively lower signal in some areas such as the temporal poles and occipital lobe (macaque), the SNR values are quite high. Previous papers have used a whole-brain average of 100 as a cut-off for study inclusion (Yeo et al., 2011) and in our averaged maps, generally every voxel exceeds this value suggesting reliable signal estimates.

Correlation matrices

The mean time signal for each seed region (within species) was obtained by averaging the BOLD time series across all voxels contained within the seed. A cross correlation matrix between all regions was then calculated for each scan while partialling out the average white matter (WM) and cerebral spinal fluid (CSF) time series in addition to six motion parameters. Following a Fisher z-score transformation to normalize the correlation values, the average pair-wise connectivity across scans (in the case of monkeys) and then subjects was calculated and then transformed back into correlation values.

Hierarchical clustering

The standard Euclidean distance between each pair of group-averaged correlations was computed to assess the similarity among the seed regions. A hierarchical cluster tree, referred to as a dendrogram,

was then derived by applying the unweighted average distance method to the distance matrix (Michener and Sokal, 1957) to allow for the relationships between the elements to be visualized. The parameters for clustering as well as its success (Supplemental Table 1) were evaluated using the cophenetic correlation – a measure of how faithfully the resulting cluster tree represents the dissimilarities among observations – for the resulting cluster trees. Hierarchical clustering does not require the a priori selection of the cluster number. However, to determine cluster assignments, a distance threshold must be chosen – combining linked elements below that value into clusters. It is also important to note that the clustering will force elements (i.e., seeds) to be eventually linked together at some level. Based on consistency in the linkages within the hemispheres of each species a threshold value of 4.4 and 5.5 was used for humans and monkeys, respectively to divide the ROIs into four clusters.

Divisions of the data were also examined by evaluating the height of each link in the dendrogram with the heights of neighboring links below it in the tree producing a measure of (in)consistency. Inconsistent links are those whose height differs noticeably from the height of the links below it, indicating a possible division in the data. At an inconsistency coefficient greater than 1.1, each of the four clusters was separated from one another supporting our distance threshold. Increasing this value to the maximal inconsistency value for each set of seed regions (~1.15), after which no divisions existed, suggested a possible fifth cluster – dividing within and never between the four original clusters defined by the distance cutoff. The posterior POS (green) cluster of the left and right hemisphere of humans and right hemisphere of the monkey divided into its two main groupings and the middle aPOS (blue) cluster of the left hemisphere of the monkey split into two.

Seed-based functional connectivity

The extracted time course of each seed ROI was used as a predictor in a regression model for multiple regression at the individual participant level in which nuisance covariates for WM, CSF, and six motion parameters were included. The outputs are individual maps of predicted voxels for each regressor. In monkeys, functional connectivity maps across the scans for each monkey were calculated using a second-level fixed-effects analysis. Next, a group-level analysis was then carried out within species using a fixed-effects model producing z-score maps of connectivity associated with each seed ROI. A cluster-level network analysis was then computed across group-level seed-based networks (of a single hemisphere) encompassed by each cluster identified with the average-link clustering algorithm (fixed effect, $z > 2.3$; cluster significance: $P < 0.05$, corrected). The analysis allowed the calculation of shared functional connectivity across each of the cluster's subnetworks. In other words, functionally connected brain areas that are common across the individual seeds for all of the identified seeds in a given cluster will be revealed. Statistical differences between each cluster-level network (within a hemisphere) were also computed (fixed effect, $z > 2.3$; cluster significance: $P < 0.05$, corrected) for each species (the results of the latter analysis are shown in the supplemental material).

Images were thresholded using clusters determined by $z > 2.3$ (monkey) and $z > 3.9$ (human) and a (corrected for multiple comparisons) cluster threshold of $p < 0.05$. These different statistical thresholds (i.e., z-values) were implemented to account for differences in the sample sizes used. The group z-scores were projected from volume data to the F99 (monkey) and PALS-B12 (human) cortical surfaces (Van Essen, 2005) using the CARET (<http://www.nitrc.org/projects/caret>) enclosed-voxel method (Van Essen et al., 2001). For the sake of clarity and interpretation, voxels that were negatively correlated with the ROI time courses are not displayed in the figures or discussed. These are, however, accounted for in the cross-correlation matrix of ROI time series and whole-brain FC patterns and included in the clustering analysis.

Voxel-wise clustering

To examine the dependency of our cluster divisions on the selected seed ROIs that can make precise border definition difficult, parcellation of mPOC was further carried out at the voxel level for each hemisphere separately. A cortical gray matter mask was created in both species. In both the human and monkey, the mask encompassed 1) voxels along the entire anterior-most bank of the occipital lobe, bordered by the calcarine sulcus inferiorly; 2) posterior voxels within the precuneus, bordered anteriorly by the precuneal sulcus (Margulies et al., 2009) and inferiorly by the corpus callosum. The lateral boundary of all the aforementioned voxels was with respect the posterior-most medial wall of the intraparietal sulcus.

Within mPOC temporal parcellation. Examining relationships of spontaneous BOLD time courses within a given region of cortex can identify segregated functional clusters (e.g., Johansen-Berg et al., 2004) without the need of a priori defined seed regions. Following the same procedure described above to calculate the cross correlation matrix of the 36 seed ROIs, a group averaged correlation matrix was computed for all GM voxels within the masked region separately for each species. Hierarchical clustering was used to cluster the matrix into 4 clusters (based on the ROI cluster results). All voxels contained within each cluster assignment were then projected from volume data to the cortical surface as described above.

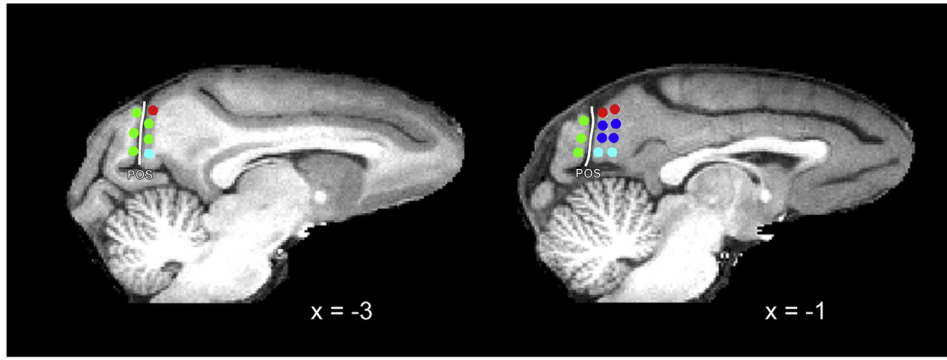
Whole-brain spatial parcellation. To evaluate the cluster divisions based upon extrinsic functional connectivity patterns that take into account the position of a voxel/region within the broader context of the network of areas in which it is embedded (e.g., Cohen et al., 2008; Hutchison et al., 2014b), a voxel-wise clustering was performed on connectivity fingerprints derived from an existing parcellation scheme. In the monkey, the F99-template normalized Lewis and van Essen (2000a,b) divisions were used to define 174 (87 per hemisphere) cortical regions of interest. In the human the Automated Anatomical Labeling (AAL, Tzourio-Mazoyer et al., 2002) atlas in MNI space was used to define 90 cortical and subcortical (45 per hemisphere) regions of interest. Each voxel defined with the mPOC mask was correlated with the mean signal of voxels within each predefined region and a group average fingerprint for each voxel was calculated. Hierarchical clustering was performed, and based on the ROI clustering results, 4 clusters were extracted. All voxels contained within each cluster assignment were then projected from volume data to the cortical surface as described above.

Results

Seed-based clustering analyses

To study the FC of mPOC, we first performed a seed-based rs-fMRI analysis on data obtained from both humans (using a 3-T scanner) and macaque monkeys (using a 7-T scanner; see [Materials and methods](#)). For both species and both hemispheres, we placed parallel rows of spherical seeds (18 in total) both posteriorly and anteriorly to the POS at two different depths in the midsagittal plane (medial and lateral) (see [Fig. 2A](#)). Note that we only report the left hemisphere results in this main manuscript; the results of the right hemisphere analyses are provided in the supplemental material for comparison. The complete correlation matrix associated with all of mPOC seed ROI time courses is shown in [Fig. 2B](#). Following average-linkage hierarchical cluster analysis of the matrix, a cluster separation of 4.4 in the human and 5.5 in the macaque could be used to distinguish 4 major clusters ([Fig. 2C](#)). Though the selection of this cutoff threshold is subjective (see [Discussion](#) for our treatment of this issue), this cluster number selection is supported by previous functional subdivisions of cells in the macaque monkey (e.g., Gamberini et al., 2011) and cytoarchitectonic

A Seed Regions



B Associated Whole-Brain Networks

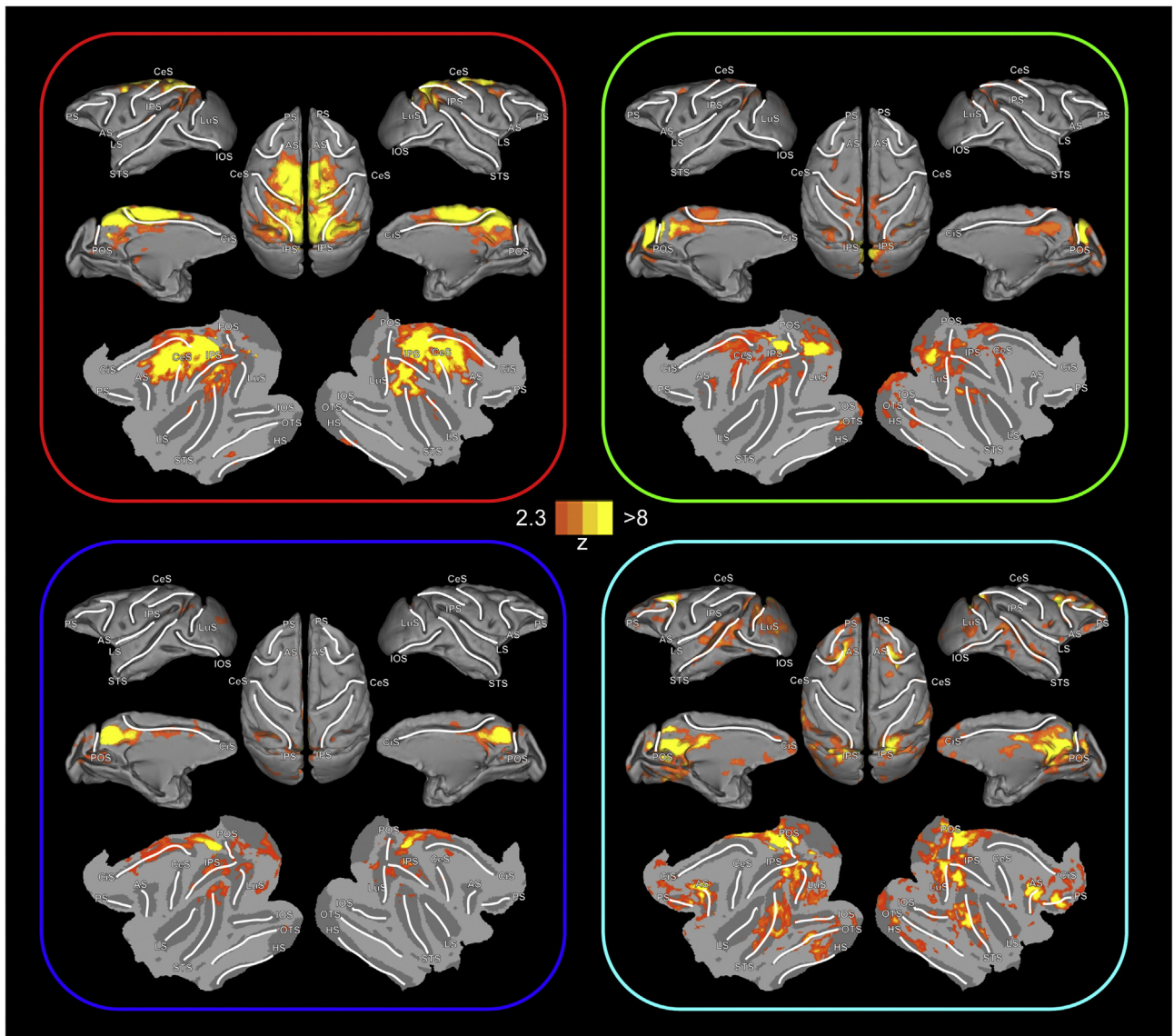


Fig. 3. Networks representing the shared connectivity of macaque monkey left hemisphere mPOC seed ROIs within each identified cluster in Fig. 2. A) ROIs are color-coded according to their cluster assignment (see Fig. 2C). B) Cluster networks are displayed on medial, lateral, dorsal and flat-map cortical representations for both hemispheres. Activation maps depict the whole-brain functional connectivity networks of the seed ROIs identified as being part of each cluster (at $z > 2.3$; $P < 0.05$, cluster-threshold corrected), normalized to the space of the F99 template (van Essen, 2004). Border colors denote the linkage between the specific activation maps shown in B and the seed ROIs shown in A. White lines indicate major sulci. Ces = central sulcus; Cis = cingulate sulcus; Hs = hippocampal sulcus; IOS = inferior occipital sulcus; LuS = lunare sulcus; OTS = occipitotemporal sulcus; STS = superior temporal sulcus; POS = parieto-occipital sulcus; PS = principal sulcus; AS = arcuate sulcus; IPS = intraparietal sulcus.

divisions (e.g., Brodmann, 1909; Brodmann and Gary, 2006), and intrinsic patterns of whole-brain FC (e.g., Yeo et al., 2011) in the human (Fig. 1). The four identified mPOC clusters were found to have good spatial differentiation within and across the anterior and posterior POS (though the spatial separation in the lateral seeds of the macaque did not follow sulcal borders, see green cluster in Fig. 2A) and was generally consistent across both hemispheres. The average-link partitioning scheme was then used to examine the shared functional connectivity among the seeds of each cluster for each species. Fig. 3 displays the results for the macaque with statistical comparisons between cluster maps shown in Supplementary Figs. 5–6. Human maps are displayed in Fig. 5 and the corresponding statistical comparisons are shown in Supplementary Figs. 8–9.

Dorsal aPOS (red cluster)

In the macaque, the dorsal anterior seed cluster (seeds 4, 8, and 12; red) showed positive correlations with a range of brain areas in parietal, temporal and frontal cortices. Among these areas was bilateral FC with the angular gyrus (AG) and supramarginal gyrus (SMG), medial and lateral intraparietal sulcus (IPS), superior parietal lobe (SPL), post- and precentral gyrus, cingulate gyrus, and fusiform gyrus. The majority of these areas have been implicated in various aspects of sensorimotor planning and control (for review, see Andersen and Cui, 2009) as well as spatial attentional processing (for reviews, see Moore et al., 2003; Bisley and Goldberg, 2010). Notably, much of this network resembles the somatomotor network that was previously observed with seeds placed in the macaque central sulcus (Vincent et al., 2007, see their Supplementary Fig. 2). For the right hemisphere, the clustering of seeds and corresponding profile of whole-brain FC were virtually identical (see Supplementary Fig. 4).

In the human, the dorsal anterior seed cluster (seeds 4, 8, 11, and 12; red), in contrast to that observed in the macaque, showed unilateral positive correlations with a range of brain areas in occipital, parietal, temporal, and frontal cortices. Among these areas was ipsilateral FC with the AG and SMG, lateral IPS, and precentral gyrus (with intersections of activity at the SFS and IFG—areas frequently identified in fMRI sensorimotor tasks as FEF/PMd and PMv, respectively) (Silver et al., 2005; Beurze et al., 2007; Cavina-Pratesi et al., 2010), and bilateral FC with POS, paracentral lobule, medial temporal gyrus (MTG), medial IPS, SPL, and fusiform gyrus. In many ways, this network resembles the frontoparietal and dorsal attention networks involved in the preparation of goal-directed actions and spatially directed attention (for reviews, see Corbetta and Shulman, 2002; Culham et al., 2006; Culham and Valyear, 2006; Silver and Kastner, 2009; Filimon, 2010) and corresponds well with the frontoparietal control and dorsal attention networks observed in previous whole-brain parcellations (cf. Power et al., 2011; Yeo et al., 2011). Notably, in contrast to the macaque, we did not find any statistically significant FC with somatomotor cortex (i.e., somatosensory and motor cortex). For the right hemisphere, the clustering of seeds and corresponding profile of whole-brain FC was near identical. It is worth recognizing that, of all the clusters explored (for comparison, see below), the seed cluster assignment for this dorsal aPOS subdivision, for both the human and macaque, and across the hemispheres within each species, was the most consistent.

Middle aPOS (blue cluster)

In the macaque, the middle aPOS seed cluster (seeds 2, 3, 6, 7; blue) showed positive correlations with bilateral occipital cortex, cingulate gyrus, precentral gyrus, medial IPS, AG, and SMG. Notably, for the right hemisphere, we observed a slightly different arrangement of seed clustering for the middle aPOS (which instead contained seeds 3, 7, 11, 15, 18), and a more extensive associated

network of FC (Supplementary Fig. 4). Specifically, in addition to the areas found with left hemisphere middle aPOS, the right hemisphere middle aPOS cluster was additionally found to be functionally connected with left and right somatomotor cortices, and some right-lateralized areas like the medial frontal gyrus and hippocampus, and the right inferior frontal gyrus.

In the human, the middle aPOS seed cluster (seeds 3 and 7; blue) showed positive correlations with several bilateral frontoparietal areas. Among these was bilateral FC with anterior posterior cingulate cortex (PCC), AG, SMG, superior and middle frontal gyri, cingulate gyrus, and ipsilateral FC with the fusiform gyrus, MTG, and inferior frontal gyrus. Despite the clustering of seeds being slightly different for the right hemisphere (i.e., seeds 3, 7 and 10 were clustered together), the profile of whole-brain FC was near identical (see Supplementary Fig. 7).

Ventral aPOS (cyan cluster)

In the macaque, this seed cluster (seeds 1, 5, and 9; cyan) showed positive correlations with several areas of occipital, parietal, temporal, and frontal cortices. Among these was bilateral FC with the occipital lobe, posterior cingulate, inferior temporal and superior temporal gyri, AG, SMG, superior, middle and inferior frontal gyri and the medio-orbital gyrus. Notably, despite the clustering of seeds being slightly different for the right hemisphere (i.e., seeds 1, 2, 5, 6, 9, and 10 were clustered), the profile of whole-brain FC was near identical (see Supplementary Fig. 4).

In the human, this seed cluster (seeds 1, 2, 5, 6, 9, and 10; cyan), in contrast to that observed in the macaque, showed largely unilateral positive correlations with a range of brain areas in occipital, parietal, temporal and frontal cortices. Among these, there was ipsilateral FC with PCC, fusiform gyrus, AG, and SMG, anterior superior and middle temporal gyri, superior and middle frontal gyri and medial frontal pole. This network of activity closely corresponds to that frequently associated with the classic default network (Buckner et al., 2008). Despite the clustering of seeds being slightly different for the right hemisphere (seeds 1, 2, 5, 6, and 9 were clustered), the profile of whole-brain FC was nearly identical, with the exception that we did observe more bilateral FC, particularly with the fusiform gyrus, anterior superior temporal gyrus, and superior frontal gyrus.

Posterior POS (green cluster)

In the macaque, this seed cluster included seeds along the medial posterior bank of the POS as well as the lateral posterior and anterior banks of the POS (i.e., seeds 10, 11, and 13–18; green). It showed positive correlations with a largely symmetrical bilateral network, which included the occipital lobe, AG, SPL, medial postcentral gyrus, and fusiform gyrus as well as ipsilateral precentral gyrus. Despite the clustering of seeds slightly differing for the right hemisphere (i.e., seeds 13, 14, 16 and 17), we observed a largely similar bilateral pattern of whole-brain FC with the addition of some other sites of FC, such as the left inferior temporal gyrus and parahippocampal gyrus.

In the human, we found that the clustering of seeds greatly differed from that of the macaque, and was entirely limited to the posterior bank of the POS (seeds 13–18). Correspondingly, it showed positive correlations that were almost entirely constrained to bilateral occipital cortex. The exception to this was that we observed very small areas of FC in ipsilateral medial IPS and SPL, precentral gyrus, and contralateral superior frontal gyrus. For the right hemisphere, the clustering of seeds was identical. The associated whole-brain FC maps, however, slightly differed in that the small areas of FC that extended outside of occipital lobe were along the ipsilateral superior temporal gyrus and precentral gyrus.

Convergence in networks associated with the separate mPOC clusters

To visualize where in the brain the different mPOC clusters show mutual versus distinct patterns of whole-brain FC, we overlapped the FC maps associated with each of the mPOC subdivisions defined by

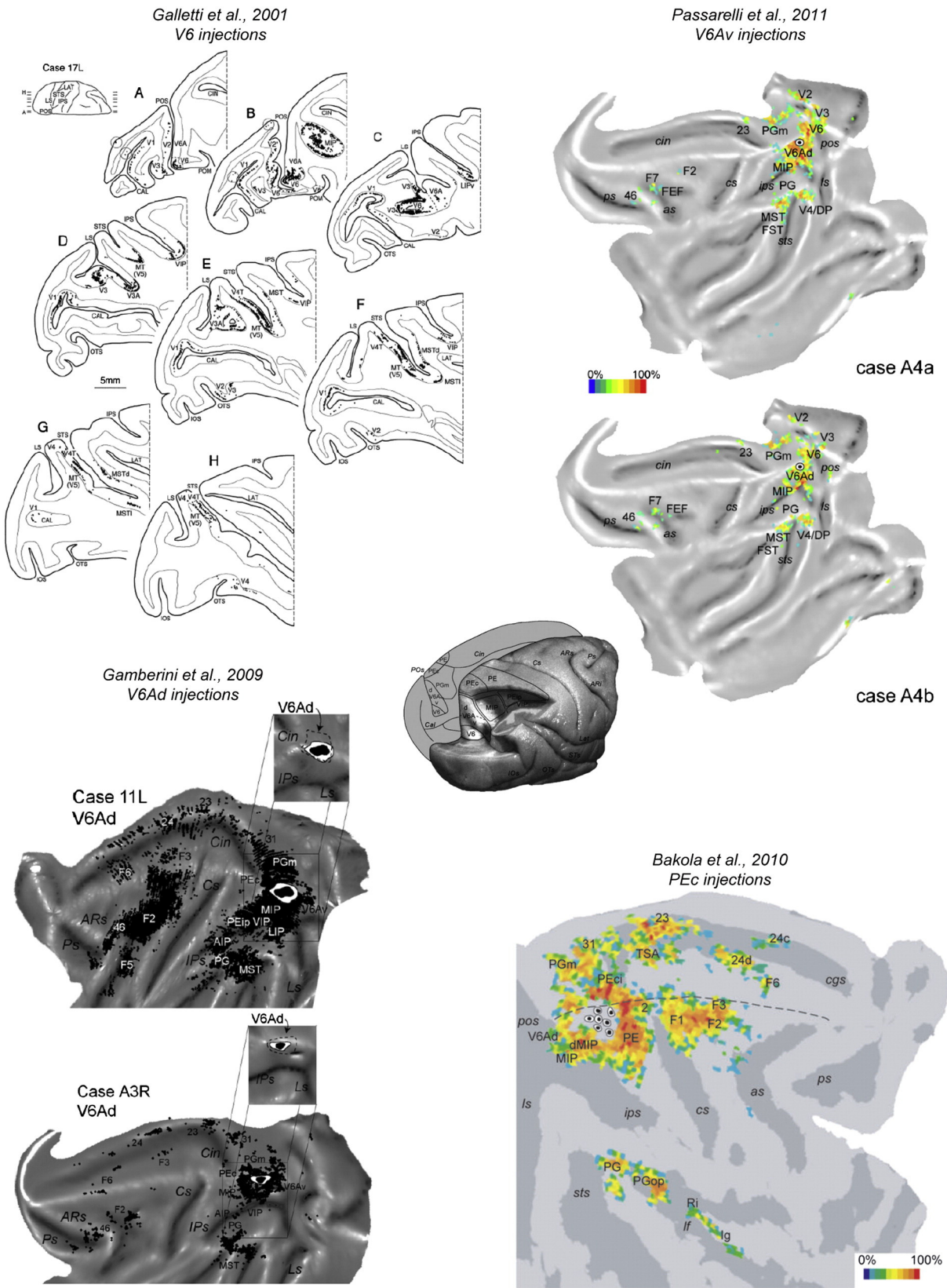


Fig. 4. Previous results of retrograde neuroanatomical tracer studies in macaque mPOC. Top left, cortical distribution of labeled cells after V6 tracer injections (represented by black dots) shown on parasagittal sections taken at the levels shown on the brain silhouette (top left; image taken from Galletti et al., 2001). Top right, cortical distribution of labeled cells after V6Av tracer injections (represented as a color density map, expressed as a percentage of maximum value obtained throughout cortex) shown on two-dimensional reconstructions (image taken from Passarelli et al., 2011). Bottom left, cortical distribution of labeled cells after V6Ad tracer injections (represented by black dots) shown on two-dimensional reconstructions (image taken from Gamberini et al., 2009). Bottom right, cortical distribution of labeled cells after PEc tracer injections (represented as a color density map, expressed as a percentage of maximum value obtained throughout cortex) shown on two-dimensional reconstructions (image taken from Bakola et al., 2010). To provide reference for the sites of tracer injections in mPOC, a macaque brain with labeled cytoarchitectonic boundaries is shown at centre (image taken from Gamberini et al., 2009).

hierarchical clustering (see Fig. 6). There are striking differences in the lateralization of the FC maps associated with the human compared to macaque brain. That is, as noted in the sections above, for each seeded hemisphere we find a largely bilateral and symmetrical pattern of whole-brain FC in macaques, whereas in humans, we found a much more ipsilateral pattern of whole-brain FC. Also apparent is the consistency in the areas of network convergence across mPOC subdivisions within each species. That is, in the macaque, all mPOC clusters show FC with bilateral precuneus, PCC, inferior parietal cortex (the AG and SMG), the superior-most STS and the precentral gyrus (just posterior to the arcuate sulcus). In the human, like the macaque, all mPOC clusters show FC with ipsilateral PMC and inferior parietal cortex (the AG and SMG). However, as a departure from that observed in the macaque, we instead find convergence zones in the left middle temporal gyrus and the left superior frontal gyrus (for the left hemisphere mPOC clusters only). This may reflect, to some extent, a by-product of some of the functional hemispheric specialization that characterizes much of human cortex. For example, evidence in humans suggests that the left hemisphere may be particularly specialized for the visual–motor control of action (Serrien et al., 2006) as well as speech processing and communicative behavior (Hickok and Poeppel, 2000; Davis and Johnsrude, 2003; Hickok and Poeppel, 2007), and these processes may be particularly well developed in the right-hand dominant participants tested here.

Comparisons between species of mPOC network laterality

To examine the extent to which species-specific differences exist in the laterality of mPOC functional networks, we contrasted FC maps associated with all the left versus right hemisphere seeds (and vice versa). The results of these direct hemispheric comparisons are shown in Fig. 7. There is strikingly more robust and extensive patterns of ipsilateral FC in human compared to macaque cortex. This demonstrates that the FC networks associated with mPOC seeds are largely bilateral in the macaque monkey and primarily unilateral in humans. This general observation can be made, though it is not as explicit, from visual comparisons of Figs. 3 and 5.

Voxel-wise cluster analyses

In addition to the seed-based analyses, we performed two clustering analyses of the mPOC region at the voxel-wise level. The first of these analyses clustered mPOC voxels according to the intrinsic temporal relationships that these voxels have with each other (i.e., within-mPOC temporal parcellation). The second of these analyses clustered mPOC voxels according to relationships in their associated spatial connectivity fingerprints (i.e., whole-brain spatial parcellation). Thus, in the case of the first voxel-wise analysis, hierarchical clustering will be driven by similarities in the individual timecourses of the mPOC voxels themselves; in the case of the second voxel-wise analysis, hierarchical clustering will be driven by similarities in the distributed spatial maps associated with each individual mPOC voxel. The results of these two separate analyses are shown in Fig. 8 and the center of mass of each cluster is listed in Supplemental Table 2.

What can be immediately observed is the striking level of convergence in the parcellation results of the within mPOC temporal parcellation (Fig. 8A) and the whole-brain spatial parcellation (Fig. 8B) not just within each species (compare within the columns of Fig. 8A and B), but also between the species (compare across the columns of Fig. 8A and B). That is, in both the macaque and human, we find that mPOC can be reliably subdivided into a dorsal–ventral gradient and a posterior–anterior gradient. This dorsal–ventral gradient is found anterior to the POS, is composed of a dorsal, middle, and ventral region, and reasonably corresponds to the subdivisions found with our seed-based analyses (compare Fig. 8 with Fig. 2A). By contrast, the aforementioned posterior–anterior subdivision extends across the POS, with the

cortex posterior to the POS generally forming one cluster and the cortex anterior to the POS being comprised of the other three clusters. On this note we do recognize that the posterior–anterior voxel-wise clustering in the macaque is blurred across the POS, with some portion of the voxels anterior to the POS being clustered with voxels posterior to the POS. This is consistent with the parcellation results of our seed-based analyses. Nevertheless, in general, these dorsal–ventral and posterior–anterior gradients can be easily observed. Importantly, we found that clustering based on hierarchical versus k-means algorithms did not significantly alter this general topography (see Supplementary Fig. 10). For the sake of comparison, we also examined a finer number of partitions (an 8-cluster solution). Here, we not only observed a clustering that differed between species (see Supplementary Fig. 11) but one that also markedly departs from previous subdivisions of the area based on cytoarchitectonics, patterns of cortico-cortical connectivity, or neuronal response properties (for example, see Figs. 1 and 4 for comparison). For these reasons, we believe that much more tractable interpretations can be applied to the 4-cluster solution presented here. When we applied the same temporal and whole-brain parcellation schemes to the right hemisphere, we found good correspondence with those observed here (see Supplementary Fig. 12), with the exception that the within mPOC temporal parcellation in the macaque provides a differentiation of clusters in the medial–lateral plane (with the posterior medial wall of the IPS, MIP, being assigned its own cluster).

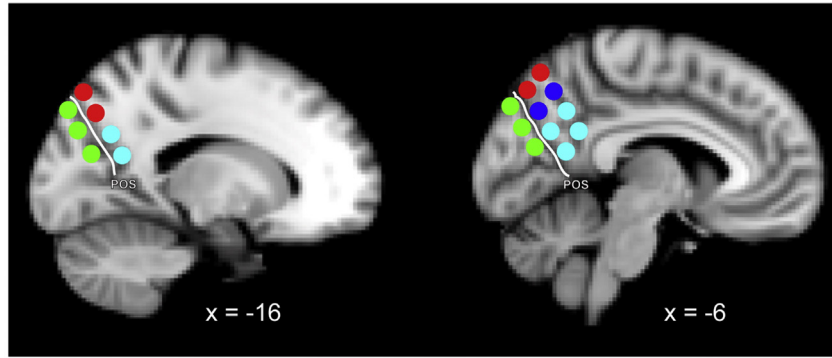
Discussion

Here, we clustered both seed regions and individual voxels in the mPOC of the human (collected at 3T) and macaque monkey (collected at 7T) based on the group-averaged FC patterns associated with spontaneous BOLD correlations of rs-fMRI data. We first employed a seed-based hierarchical clustering approach on the time course correlations within mPOC in order to determine coarse functional boundaries. We then examined the shared whole-brain network FC associated with each of these mPOC clusters. This data-driven approach permitted identification of four broad and spatially separated clusters that corresponded with graded differences in whole-brain FC patterns. Specifically, we found that both macaque and human mPOC varied systematically along the dorsal–ventral axis anterior to the POS and along the posterior–anterior axis across the POS. To bolster these seed-based results, we then performed a more fine-grained voxel-wise clustering analysis based either on the pattern of within mPOC temporal correlations or on the pattern of distributed whole-brain spatial correlations associated each mPOC voxel. In addition to supporting the clustering results of our seed-based analyses, we found that the two separate voxel-wise clustering approaches tended to converge upon similar parcellation solutions. This suggests that the functional parcellations in both macaque and human are tightly linked to the distinct patterns of whole-brain functional connectivity (Fig. 9).

Current results in the context of emerging structural–functional subdivisions of mPOC

Previous studies of anatomical connections in NHPs reported a general posterior-to-anterior transitional gradient within the precuneus, suggestive of 3 separable, homogeneous regions: 1) a posterior portion, PO, exhibiting prominent connectivity with visual areas (Colby et al., 1988); 2) a middle portion, PGm, exhibiting prominent connectivity with cognitive/associative brain areas like STS, IPL, and DLPFC (Pandya and Seltzer, 1982; Leichnetz, 2001; Morecraft et al., 2004; Buckwalter et al., 2008) and, 3) an anterior portion, PEc, exhibiting prominent connectivity with medial somatosensory and motor regions (Morecraft et al., 2004; Bakola et al., 2010). However, more recent functional and anatomical evidence has suggested that the posterior precuneus (area PO), in particular, is itself quite heterogeneous, being loosely comprised of three distinct sub-regions, topographically organized ventrally-to-dorsally: V6, V6Av, and

A Seed Regions



B Associated Whole-Brain Networks

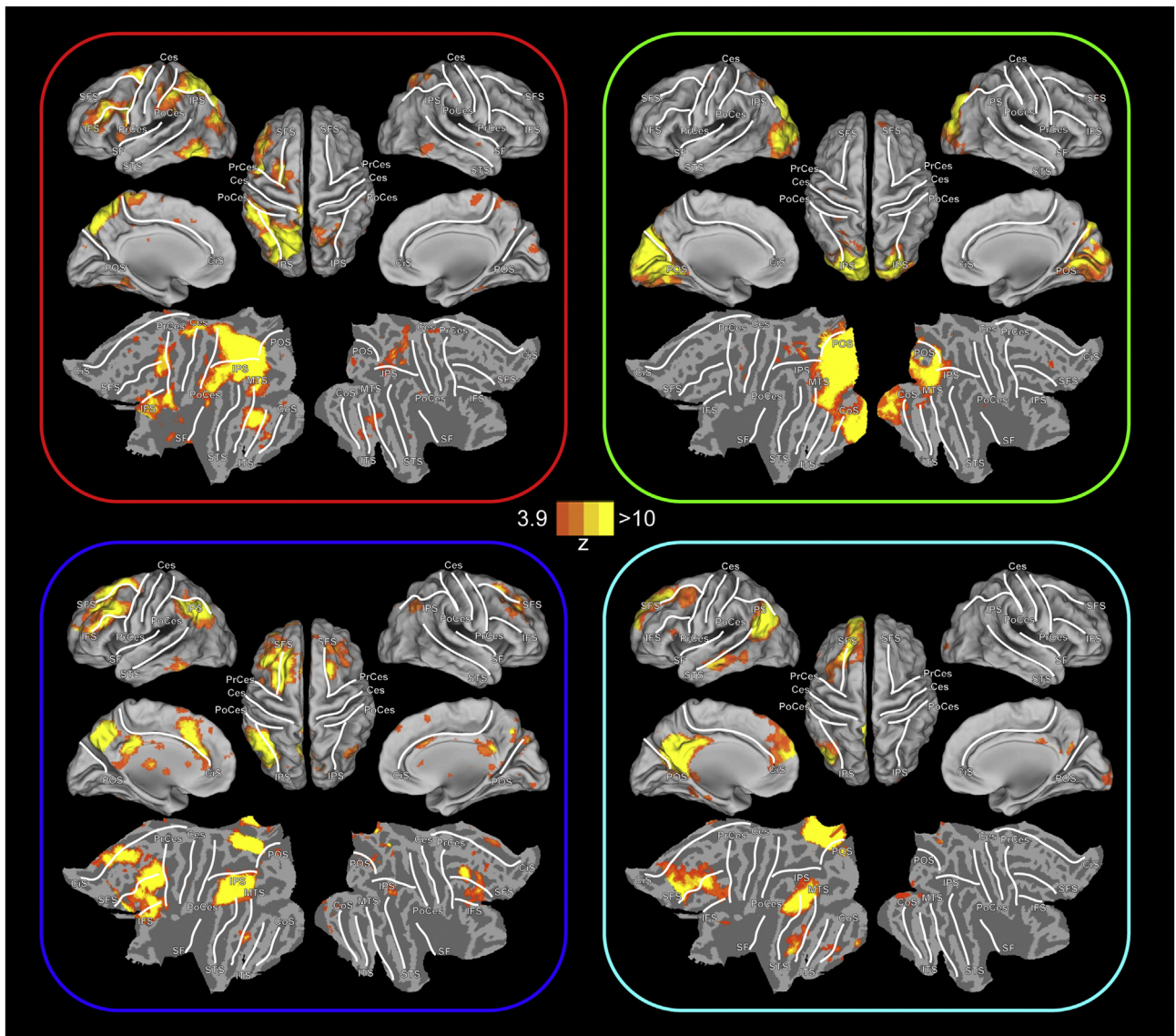


Fig. 5. Networks representing the shared connectivity of human left hemisphere mPOC seed ROIs within each identified cluster in Fig. 2. A) ROIs are color-coded according to their cluster assignment (see Fig. 2C). B) Cluster networks are displayed on medial, lateral, dorsal and flat-map cortical representations for both hemispheres. Activation maps depict the whole-brain functional connectivity networks of the seed ROIs identified as being part of each cluster (at $z > 3.9$; $P < 0.05$, cluster-threshold corrected), normalized to the space of the PALS-B12 template (Van Essen, 2005). Border colors denote the linkage between the specific activation maps shown in B and the seed ROIs shown in A. White lines indicate major sulci. Ces = central sulcus; Cis = cingulate sulcus; CoS = collateral sulcus; IFS = inferior frontal sulcus; IPS = intraparietal sulcus; ITS = inferior temporal sulcus; MTS = middle temporal sulcus; PoCes = postcentral sulcus; POS = parieto-occipital sulcus; PrCes = precentral sulcus; SF = sylvian fissure; SFS = superior frontal sulcus; STS = superior temporal sulcus.

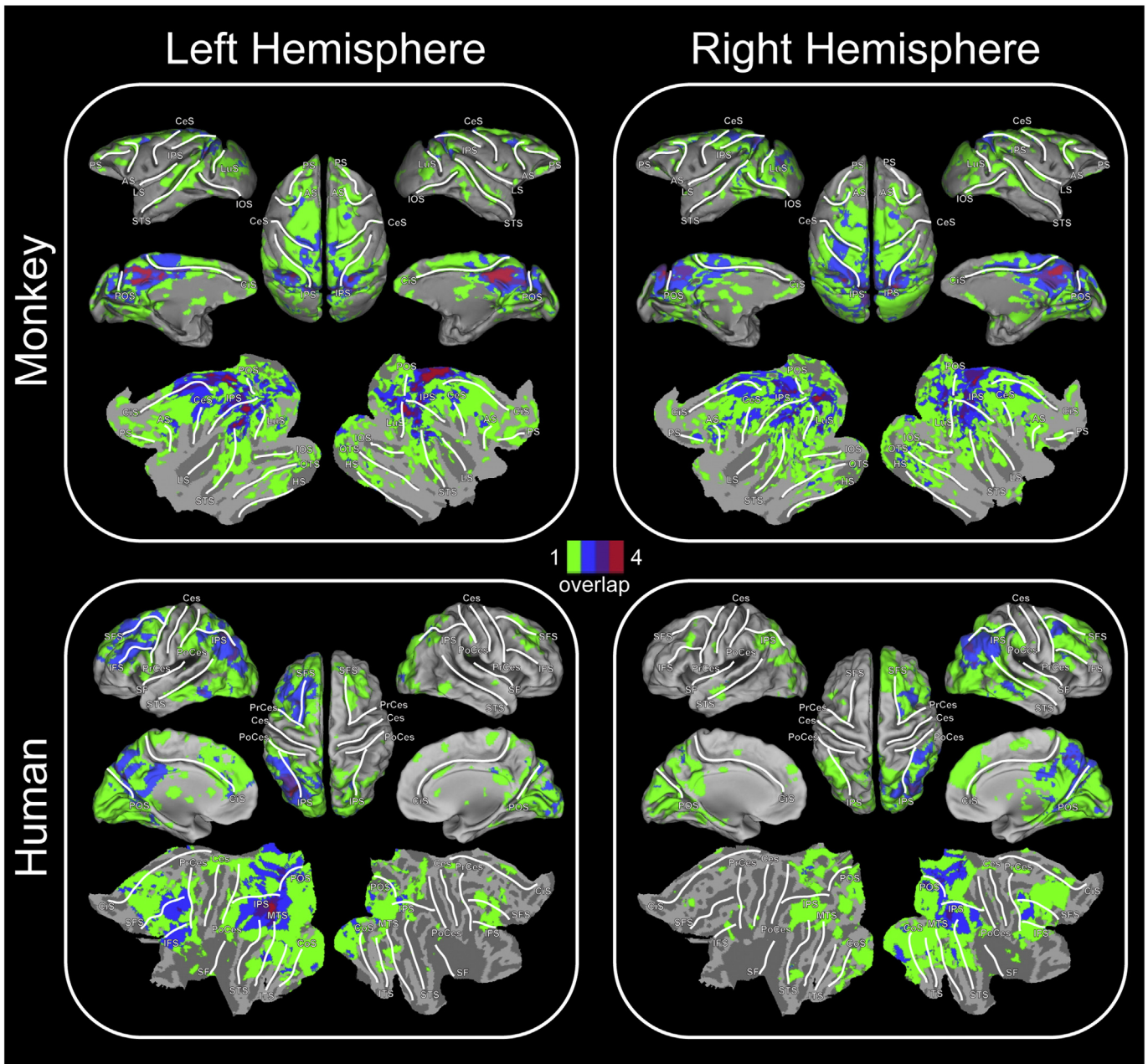


Fig. 6. Conjunction analysis across the functional connectivity maps of all mPOC clusters. Color maps represent the number of mPOC functional maps that have significant (z -score > 2.3 , monkey; z -score > 3.9 , human) FC at each voxel, thus identifying the core regions that show FC with all mPOC clusters. For interpreting which seed-based mPOC clusters are driving the overlap effects, see Figs. 3 and 4 (and Supplementary Figs. 4 and 7).

V6Ad. Region V6 is a pure visual area, receives direct projections from V1 and exhibits connectivity with MT. Consistent with this, the area is retinotopically organized and contains cells responsive to motion (Galletti et al., 1999). In contrast, region V6A, which has recently been cytoarchitecturally subdivided into a ventral and dorsal component (i.e., V6Av and V6Ad, respectively, Luppino et al., 2005), contains cells with both visual and motor response properties as well as cells responsive to arm movements in the absence of any vision (motor-type cells, see Fattori et al., 2001; Fattori et al., 2005; Gamberini et al., 2011). In further support of this recent cytoarchitectonic subdivision of V6A, V6Ad predominantly shows connections with areas of parietal (MIP, PEc, and medial PG) and premotor cortex (PMd) and shows comparatively more somatosensory-type neuronal responses than V6Av. By contrast, V6Av predominantly shows connectivity with non-primary visual areas,

including V6, as well as parietal cortex, has much more sparse connections with frontal cortex, and shows comparatively more visual-type responses than V6Ad (Gamberini et al., 2009; Gamberini et al., 2011; Passarelli et al., 2011). Causal evidence for the role of V6A in visuomotor transformations for action comes from the variety of specific deficits in reaching, wrist orientation, and grasping that can be observed when lesions or inactivation are delivered to the anterior bank of the POS in NHPs (Battaglini et al., 2002; Hwang et al., 2012). It is worth noting that, in addition to areas V6, V6Av, and V6Ad, the very caudal extent of area PEc also directly abuts the dorsal-most portion of the POS. Fluorescence tracer studies show that it receives projections from a network of parietal, mesial, and frontal areas, the latter mainly being the dorsocaudal part of premotor area F2 (Bakola et al., 2010). Consistent with this pattern of connectivity, electrophysiological recordings show

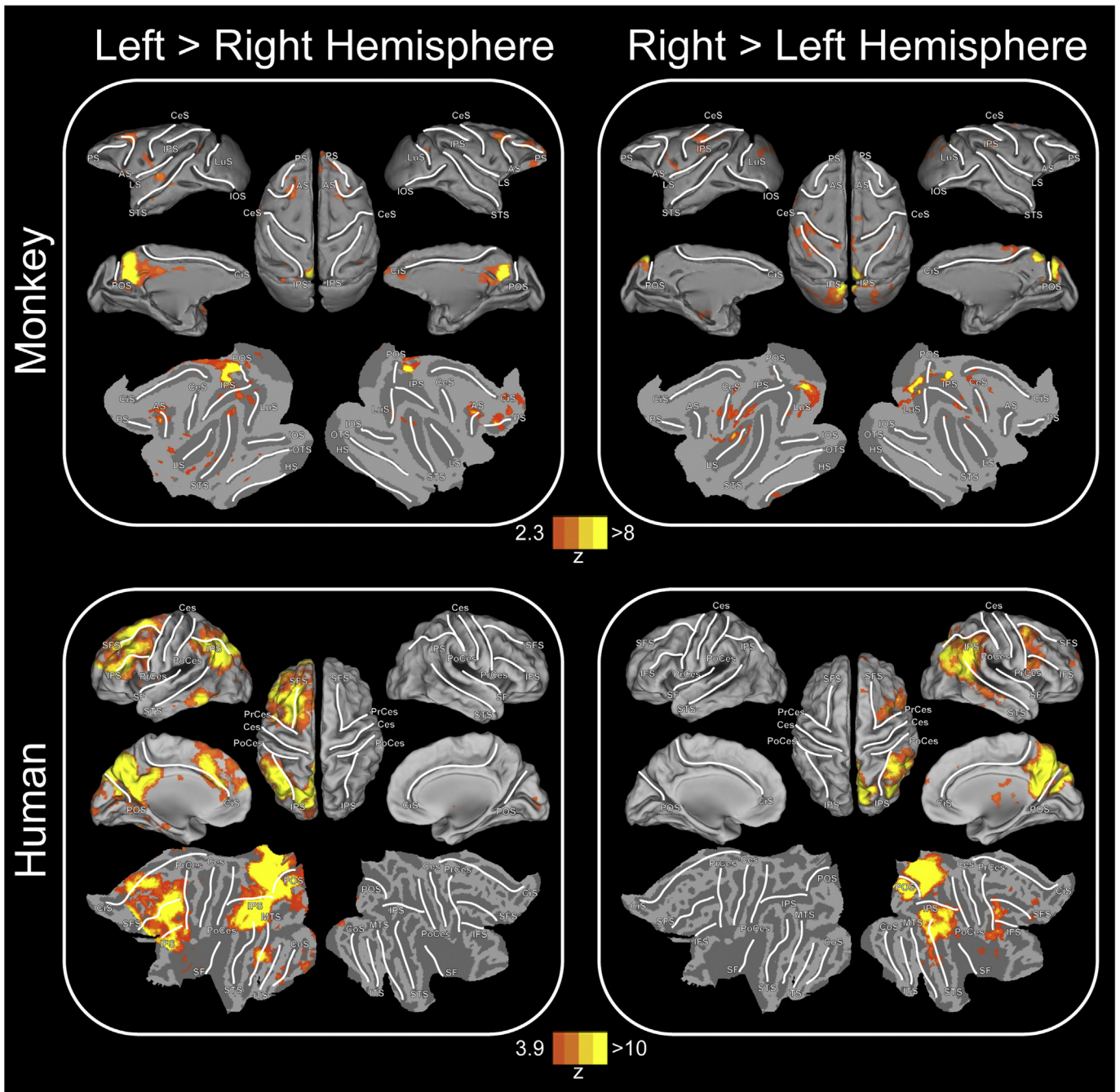


Fig. 7. Comparison of laterality in mPOC functional connectivity maps across all seed regions in the macaque monkey and human. Activation maps depict contrasts of the functional connectivity networks associated with all the left vs. right hemisphere seeds (left panels) and all the right vs. left hemisphere seeds (right panels) for both the macaque monkey (top panels) and human (bottom panels). Maps are statistically thresholded for each species according to the color bars shown at center. White lines indicate major sulci in accordance with Fig. 3 and 5 captions.

that both oculomotor and reach-related tasks elicit robust activity in PEC neurons (Battaglia-Mayer et al., 2001; Ferraina et al., 2001), suggestive that the region plays a prominent role in coordinated limb movements.

Based on cortical topography as well as comparisons with retrograde and bidirectional neuronal tracer studies in NHPs (see Fig. 4, Gamberini et al., 2009; Bakola et al., 2010; Passarelli et al., 2011), we submit that our macaque dorsal aPOS region (red cluster) corresponds with the connectivity patterns of V6Ad and caudal PEC. Our middle aPOS (blue cluster) and pPOS (green cluster) regions correspond with the topography and connectivity patterns of areas V6Av and V6 (and perhaps also V3A in occipital cortex, see Felleman et al., 1997; Galletti et al., 2005),

though not necessarily in a one-to-one fashion. That is, the resting network activity associated with V6 and V6Av (and also V3A) likely contributes (to differing degrees) to the FC profiles associated with each our middle aPOS and pPOS regions and, likewise, the resting network activity associated with both V6Ad and caudal PEC (but perhaps also part of V6Av) likely contributes to the FC profiles associated with our dorsal aPOS region. We suspect that the absence of a clear one-to-one mapping may be explained, at least in part, by our data-driven clusters encompassing more than one functional area (e.g., the dorsal aPOS region comprising cortex that belongs to areas V6Ad and PEC). Nevertheless, at the level of cytoarchitecture, our dorsal and middle

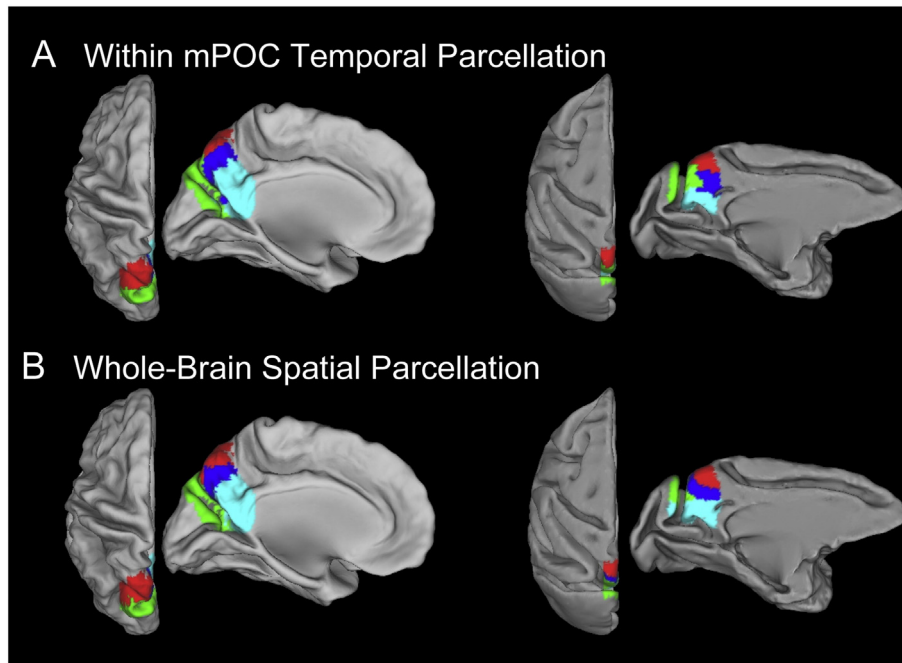


Fig. 8. Resting state-based cluster analyses of mPOC voxels in both the macaque monkey and human. A) Results of voxel cluster analysis for a 4-cluster solution, based on temporal correlations within mPOC, displayed on the dorsal and medial cortical representations of the left hemisphere in both the human (left) and macaque monkey (right). B) Results of voxel cluster analysis for a 4-cluster solution, based on spatial correlations in the whole-brain functional connectivity maps of mPOC voxels, displayed the same as in A. See Supplementary Fig. 11 for a comparison of hierarchical and k-means clustering approaches and see Supplementary Fig. 12 for the results of the 8-cluster solution.

aPOS clusters—at least in the human—appear to closely correspond to the locations of areas 7p and 7m, respectively, as recently delineated by [Scheperjans et al. \(2008a,b\)](#) in postmortem brains. As for our ventral aPOS region (cyan cluster), previous work has shown that the PCC/retrosplenial cortex exhibits prominent connections to ventral prefrontal cortex and medial temporal regions, suggestive that the area plays a role in the neural processing of emotion, motivation and memory ([Kobayashi and Amaral, 2003](#); [Parvizi et al., 2006](#); [Kobayashi and](#)

[Amaral, 2007](#); [Kravitz et al., 2013](#)). We found prominent FC with each of these areas (as well as frontal areas like FEF, which are only polysynaptically connected with PCC, [Morris et al., 1999](#)), and thus our ventral cluster likely corresponds with some of the spontaneous activity associated with PCC/retrosplenial cortex (Brodmann's areas 23 and 31, [Vogt, 2009](#)). Alongside these proposed subdivisions of mPOC, we generally find that, consistent with anterograde and retrograde tracer work of the PMC in cynomolgus monkeys ([Parvizi et al., 2006](#)), all our aPOS

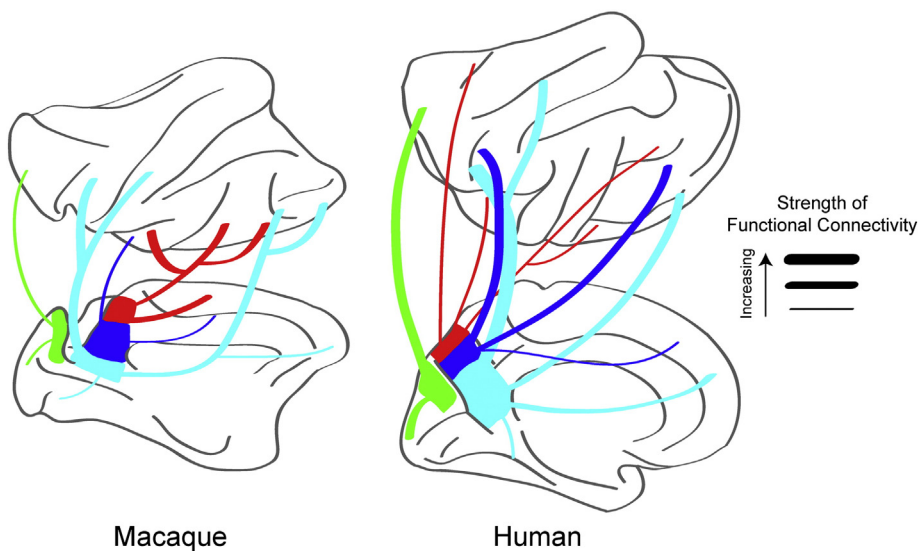


Fig. 9. Summary of functional connectivity patterns emerging from the 4 mPOC subdivisions in both the macaque monkey and human. A simplified summary of the divisions and functional connections for regions in the left mPOC is displayed on schematic lateral (top) and medial (bottom) cortical representations of the left hemisphere in both the macaque monkey (left) and human (right). Regions and their connections are color-coded according to their cluster assignment (see [Fig. 2C](#)) and meant to highlight prominent differences between divisions and species. The thickness of connections denotes the relative strength of functional connectivity (see [Supplemental Table 3](#)). To see full connection patterns, see [Figs. 3 and 5](#) for the monkey and human, respectively.

regions (dorsal, middle and ventral subdivisions) show FC both with each other and with various aspects of the anterior cingulate gyrus, DLPFC, lateral parietal cortex (AG and SMG), and STS.

Through retinotopic mapping studies in humans, putative homologues of monkey visual areas V6 and V6Av has been functionally identified (Pitzalis et al., 2006; Fattori et al., 2009a; Pitzalis et al., 2013a). Putative human V6 (hV6) is located in the posterior dorsalmost POS and hV6Av borders hV6 anteriorly within the POS (Pitzalis et al., 2010; Pitzalis et al., 2013b; Pitzalis et al., 2013a). In addition, consistent with more recent anatomical and neural investigations in the macaque monkey (Fattori et al., 2009b; Gamberini et al., 2009; Fattori et al., 2010; Passarelli et al., 2011; Fattori et al., 2012) several lines of evidence implicate the aPOS region in the preparation and execution of human hand actions. For example, consistent with SPOC playing a role in visual-to-motor transformations for arm movements, a gradient transition of functional responses can be observed: hV6Av shows greater fMRI responses for the execution of spatially directed pointing movements than V6 (Pitzalis et al., 2013a), but approximately equal responses to saccades (Tosoni et al., 2014); by contrast, hV6Ad, which is thought to border hV6Av just anteriorly (in the anterior POS), shows greater responses for pointing movements than saccades (Tosoni et al., 2014). In support of this functional neural organization, a whole host of fMRI work reports foci of activity in aPOS during the preparation and execution of reaching, pointing and grasping actions (Astafiev et al., 2003; Connolly et al., 2003; Prado et al., 2005; Filimon et al., 2009; Gallivan et al., 2009; Bernier and Grafton, 2010; Cavina-Pratesi et al., 2010; Gallivan et al., 2011a; Gallivan et al., 2011b; Monaco et al., 2011; Gallivan et al., 2013; Gallivan et al., 2015). This corresponds well with the types of reaching deficits observed in optic ataxia patients (Perenin and Vighetto, 1988; Andersen et al., 2014), many of whom have lesions to the mPOC region, near the parieto-occipital junction (Karnath and Perenin, 2005). Based on these functional response properties, it is expected that dorsal mPOC, in particular, should show positive correlations with the networks involved action planning and control and spatial orienting.

With respect to the current rs-fMRI results, the FC maps associated with the dorsal (red), middle (blue), and ventral (cyan) aPOS regions correspond with several components of the frontoparietal control, dorsal attention, and default networks associated with action planning and control (Yeo et al., 2011), the orienting spatial attention (Corbetta and Shulman, 2002), and internal modes of cognition (Buckner et al., 2008; Leech et al., 2012), respectively (see Fig. 1 for comparison). However, this mapping between aPOS subdivisions and associated networks, like that found with the macaque, does not appear to be one-to-one. For instance, rather than the FC of the dorsal aPOS (red) corresponding to just one whole-brain network, it instead shows FC with several areas that comprise both the frontoparietal control (FPC) and dorsal attention networks (DAN; see Yeo et al., 2011, see also Fig. 1). This is evidenced by dorsal aPOS showing FC with both the SPL and PMd/FEF (belonging to the DAN) as well as FC with both the IPS and middle frontal gyrus (belonging to the FPC). By contrast, the middle aPOS (blue) shows FC with several areas of the FPC and DN (see Yeo et al., 2011, see also Fig. 1). This is evidenced by FC with both the ACC and MTG (belonging to the FPC) as well as FC with PCC and superior frontal gyrus (belonging to the DN). In contrast to the FC associated with the dorsal aPOS cluster, the FC associated with the middle aPOS cluster is much more bilateral, particularly in middle and superior frontal gyrus, more lateralized in parietal cortex, and more medial in frontal cortex. This profile of FC is to be contrasted with that of the ventral aPOS (cyan) cluster, which shows FC with several hallmark structures of the classic DN (Yeo et al., 2011, see also Fig. 1). This includes FC with AG, STS, and medial prefrontal cortex. In contrast to the FC associated with the middle aPOS cluster, the FC associated with the ventral aPOS cluster is not bilateral, even more lateralized in parietal cortex, and even more medial in frontal cortex. Finally, in contrast to the subdivisions found in aPOS, for the single pPOS (green) cluster we find classic visual network activity (Yeo et al., 2011, see also Fig. 1). Taken together, this work is not

only consistent with the classic view that the medial parieto-occipital cortex is a key hub of an expansive frontoparietal pathway involved in visual spatial processing and the planning and control of actions (Ungerleider and Mishkin, 1982; Goodale and Milner, 1992), but also the more recent view that the area, by virtue of the projections it sends to the parieto-prefrontal and parieto-medial temporal pathways, plays important roles in spatial working memory and navigation, respectively (Kravitz et al., 2011).

Comparison with previous rs-fMRI parcellation in macaques and humans

The present results extend a study that used rs-fMRI in both humans and macaques to examine the intrinsic functional connectivity of the precuneus and posterior cingulate cortex (Margulies et al., 2009), in which the functional connectivity was constructed from 21 seed ROIs in the right PMC. We focused our analyses not on the entire PMC, which has also been a target of investigation in other previous human DTI (Zhang et al., 2014) and rs-fMRI work (Zhang and Li, 2012; Yang et al., 2014), but rather on the cortex that lies directly adjacent to the POS, both posteriorly and anteriorly. In this way, the present work was not motivated to explore separations in the patterns of intrinsic FC that arise along the posterior–anterior axis of entire PMC, as previously described by others (i.e., precuneus is thought to manifest a posterior-to-central-to-anterior gradient transition of visual-to-cognitive-to-somatomotor network activity; see Margulies et al., 2009). Nevertheless, we did observe some degree of consistency with the findings of Margulies et al. (2009). For instance, when we performed the temporal voxel-wise parcellation of mPOC in the macaque we found predominantly two main cluster separations along the anterior POS (our green and cyan clusters). Similar to here, these clusters were identified by Margulies et al. (2009) as having primarily visual- and limbic-like patterns of FC (respectively). Notably, similar to that reported by Margulies et al. (2009), this same analysis in the human also revealed evidence of a visual cluster in the dorsal-most aPOS (our green cluster). The convergence of these results across separate studies using the same methods (i.e., clustering based on temporal correlations within the region) clearly suggests a visual role for dorsal anterior POS in information processing. Notwithstanding these important similarities, however, we did also observe several noteworthy profiles of whole-brain FC that depart from what Margulies et al. (2009) described.

First, whereas Margulies et al. (2009) did not observe strong premotor FC associated with their posterior or central precuneal regions (see summary of their findings in Fig. 1F), which we suspect occupies our dorsal aPOS (red) region, here we find prominent premotor connectivity associated with this region in both species (and, of particular note, somatomotor activity associated with this region in the macaque). In addition, whereas Margulies et al. reported positive correlations with visual areas when seeding the posterior precuneal region (dorsal portion of the parieto-occipital fissure), we only reliably found robust visual network FC when we seeded the posterior bank of the POS (a general region not thoroughly explored by Margulies et al., 2009). Though Brodmann area 7m encompasses a fairly large expanse of precuneal cortex, our findings for the dorsal aPOS region are generally consistent with anatomical tracing studies in the cynomolgus monkey showing that area 7m, when compared to other cytoarchitectonic divisions of PMC, selectively shows connectivity with premotor (e.g., PMd) and cingulate structures as well as the SPL (Parvizi et al., 2006). Importantly, these structures are well known to be involved in the preparation and execution of hand actions (Kalaska et al., 1997; Dum and Strick, 2002; Cisek et al., 2003; Fattori et al., 2012).

Second, whereas Margulies et al. (2009) only subdivided their aPOS into a precuneal region dorsally and posterior cingulate/retrosplenial region ventrally, our analyses parcellated aPOS into 3 subdivisions, dorsal, middle and ventral. While the results of Margulies et al. (2009)

are in line with a previous parcellation of PMC that subdivided the aPOS into a dorsal visual-related network and a ventral task-negative network (Cauda et al., 2010) our parcellation results more closely conform with previous DTI-based (Zhang et al., 2014) and rs-fMRI-based PMC (Zhang and Li, 2012) and whole-brain (Yeo et al., 2011) parcellations in the human.¹

In addition to these differences in findings, there are other notable ways in which the current study adds to that of Margulies et al. (2009). First, because we examined the FC of both hemispheres (Margulies examined only the FC associated with the right hemisphere), we were able to systematically explore the degree of hemispheric lateralization observed in the mPOC FC maps for both species. Here, it is worth noting that whereas with the macaques we found a largely bilateral and highly symmetrical pattern of whole-brain FC associated with each of the left- and right-hemisphere mPOC seed clusters, in the human we typically found a largely ipsilateral organization for these same networks. This observation is in line with previous reports of differences in the resting-state networks in the two species (Hutchison et al., 2012c; Mantini et al., 2013). Second, we found that, despite the clustering of seeds for the dorsal aPOS region in both species being identical, the FC patterns associated with the dorsal aPOS (red) cluster in the human was largely limited to frontoparietal cortex, whereas in the macaque, the FC associated with this same cluster also extended into the primary somatosensory and motor cortices. This suggests that macaque and human mPOC, while generally sharing a similar functional architecture (Margulies et al., 2009) and exhibiting many of the same kinds of neural response properties (e.g., selectivity for reaching and grasping), may also exhibit some small differences in functional organization. Human precuneus comprises a significantly larger portion of brain volume than in NHPs (Cavanna and Trimble, 2006; see also Hill et al., 2010) and humans are capable of more sophisticated mentalization tasks and behaviors. It thus stands to reason that some differences in FC patterns should be expected between the species (see also Hutchison et al., 2012c; Mantini et al., 2013; Neubert et al., 2014), in spite of the fact that they exhibit similar functional and neuroanatomical organizations (Margulies et al., 2009; Mars et al., 2011; Sallet et al., 2013). Third, in addition to exploring FC associated with the medial wall of mPOC (as done in Margulies et al., 2009), we also explored FC more laterally (bounded by the posterior medial wall of the IPS, at the point where it joins the POS). This allowed us to assess any changes in cluster assignment (and associated FC) as a function of transitions in medial-to-lateral gray matter. And finally, because we additionally clustered mPOC voxels in both species according to their spatial profiles of distributed FC, we were able to qualitatively assess the degree to which temporal and spatial parcellations of mPOC converge upon common areal boundaries. We found a striking degree of convergence in both analysis approaches, suggesting that the functional subdivisions of mPOC derive their distinct temporal signatures by virtue of differences in the distributed brain areas to which they are functionally connected.

¹ Some reasons for discrepancies between our findings in macaques and humans with those of Margulies et al. (2009) may be attributed to one or more of following methodological differences: (1) We selectively focused our analysis on the cortex adjacent to the POS (both posteriorly and anteriorly) to more closely align our results with recent anatomical and functional subdivisions proposed in NHPs (Galletti et al., 1996; Galletti et al., 1999; Gamberini et al., 2009; Gamberini et al., 2011; Passarelli et al., 2011; Fattori et al., 2012) whereas Margulies et al. examined the full PMC but not the cortex posterior to the POS – this may have led to a more nuanced partitioning scheme being applied to our data; (2) The selection of our mPOC seeds and voxel-wise masks were at the group-level whereas Margulies et al. selected their seeds in MNI-normalized space at the single-subject level; (3) The observation of frontoparietal and somatomotor network activity associated with the macaque dorsal aPOS (red) region in our study may reflect the fact that our monkeys were scanned at high-field 7T, allowing for better spatial resolution, whereas Margulies et al.'s monkeys were scanned at 3T.

Methodological considerations and limitations to interpretation

Ongoing work has demonstrated that FC patterns are shaped (though not fully determined) by patterns of the underlying structural connectivity. Anatomically connected brain regions tend to show strong FC coupling, but this does not mean that FC guarantees a direct white-matter connection between the regions. This case can be made based on the current data; here we find that some of our aPOS regions in the macaque show FC with either primary visual, somatosensory, or motor cortex regions, and yet tracer studies suggest that such direct structural connections do not exist (Parvizi et al., 2006). This is in line with previous results demonstrating that the networks identified with FC measures can either reflect mono- or polysynaptic connections (Fox and Raichle, 2007; Adachi et al., 2012; Hutchison et al., 2012b; Shen et al., 2012). In addition, FC networks can be modified by repeated evoked co-activation of brain areas (Fox and Raichle, 2007; Deco and Corbetta, 2011; Deco et al., 2011) and can vary even within the period of a standard scan (for review, see Hutchison et al., 2013). Accordingly, interpreting FC patterns requires some caution and with consideration of DTI and animal-based neuroanatomical tracer studies.

With regards to the clustering analyses performed in the current study, it is worth recognizing that a limitation to any clustering approach is that the number of clusters selected is arbitrary. That is, each cluster is comprised of increasingly smaller subclusters until eventually reaching the single-voxel level. For the current work we employed Euclidean distance cutoff values that allowed for a comparable number of clusters in both the human and macaque monkey and in the left and right hemispheres. For higher (and lower) cluster numbers, this symmetry began to break down (this can be seen in Fig. 2 or Supplementary Fig. 1). While arbitrary, this cluster number corresponds well with what might be expected from previous cytoarchitectonic (Brodmann, 1909) and FC-based subdivisions of medial parieto-occipital cortex in the human (Yeo et al., 2011) and recently emerging structural and functional subdivisions of the same area in NHPs (Galletti et al., 1996; Galletti et al., 1999; Gamberini et al., 2009; Gamberini et al., 2011; Passarelli et al., 2011; Fattori et al., 2012). Nevertheless, the parcellation provided here does not preclude interpretation of more fine-grained subdivisions, which can be directly appreciated through visual inspection of our dendrograms. The delineation of smaller units, however, is inherently limited by the processes of brain normalization (to allow for comparison across the group), the spatial smoothing criteria applied (Gaussian kernel of FWHM 3 mm in the macaque and 6 mm in the human), as well as the sizes of the seed ROIs used (1 mm in the macaque and 4 mm in the human) and voxel sizes collected in each species (macaque Set 1: 1.3 mm × 1.3 mm × 1.3 mm; macaque Set 2: 1 mm isovoxel; humans: 3 mm isovoxel). All three of these factors may lead to distortions in areal boundaries (especially across the sulci), magnify hemispheric differences in FC between the species, and prevent more reliable, fine-grained parcellations of mPOC. In addition, we recognize that we can only offer qualitative comparisons of our results with those of previous tracer results in NHPs that provide a distribution of labeled cells within a single hemisphere. A quantitative assessment, at least for NHPs, will require fMRI and tracer injections in the same cohort of animals.

Lastly, it is worth noting that in our discussion of the whole-brain FC patterns associated with the different mPOC clusters, we have attempted, where appropriate, to situate our results within the context of previously published work with DTI, neuroanatomical tracing methods in animals, and task-based or rs-based fMRI. Often this entails some speculation on the nature of the cortical processes that different FC networks may support (a line of reasoning called 'reverse inference', see Poldrack, 2006). Though any speculation made using reverse inference may be limited or context-dependent (Poldrack, 2011; Hutzler, 2013), given a plethora of task- and rs-based fMRI explorations in the precuneus along with evidence from NHP neurophysiology and neuroanatomical tracing in the same region (much of this discussed

above), a good supporting basis exists for such considerations. Nevertheless, we wish to acknowledge that suggestions concerning the functional processes supported by the different networks derived via resting-state analyses remain open to interpretation.

Conclusions

Multiple analysis approaches revealed consistent functional boundaries of mPOC that correspond well with graded differences in whole-brain FC patterns. While broad similarities in mPOC organization exist, species-specific differences in functional organization between macaques and humans were evident. Taken together, the results support the notion that mPOC is a heterogeneous structure, forming a critical hub of networks involved in action planning and control, spatial navigation, and working memory whose functional role has likely changed over the course of evolution.

Supplementary data to this article can be found online at <http://dx.doi.org/10.1016/j.neuroimage.2015.04.068>.

Acknowledgments

The authors are grateful to Daniel Margulies, who provided helpful comments and feedback on previous versions of this manuscript. This work was supported by operating grants from the Canadian Institutes of Health Research (CIHR) awarded to J.C.C. (MOP84293), S.E. (MOP89785), and J.R.F. and J.P.G. (MOP126158). R.M.H. was supported by a CIHR postdoctoral fellowship. J.P.G. was supported by a Banting postdoctoral fellowship and CIHR postdoctoral fellowship. We thank Ravi Menon, Joe Gati, Sarah Hughes, Adam McLean, and Don Brien for assistance and technical support with original data collection.

References

- Adachi, Y., Osada, T., Sporns, O., Watanabe, T., Matsui, T., Miyamoto, K., Miyashita, Y., 2012. Functional connectivity between anatomically unconnected areas is shaped by collective network-level effects in the macaque cortex. *Cereb. Cortex* 22, 1586–1592.
- Andersen, R.A., Cui, H., 2009. Intention, action planning, and decision making in parietal-frontal circuits. *Neuron* 63, 568–583.
- Andersen, R.A., Andersen, K.N., Hwang, E.J., Hauschild, M., 2014. Optic ataxia: from Balint's syndrome to the parietal reach region. *Neuron* 81, 967–983.
- Astafiev, S.V., Shulman, G.L., Stanley, C.M., Snyder, A.Z., Van Essen, D.C., Corbetta, M., 2003. Functional organization of human intraparietal and frontal cortex for attending, looking, and pointing. *J. Neurosci.* 23, 4689–4699.
- Babapoor-Farrokhran, S., Hutchison, R.M., Gati, J.S., Menon, R.S., Everling, S., 2013. Functional connectivity patterns of medial and lateral macaque frontal eye fields reveal distinct visuomotor networks. *J. Neurophysiol.* 109, 2560–2570.
- Bakola, S., Gamberini, M., Passarelli, L., Fattori, P., Galletti, C., 2010. Cortical connections of parietal field PEc in the macaque: linking vision and somatic sensation for the control of limb action. *Cereb. Cortex* 20, 2592–2604.
- Battaglia-Mayer, A., Ferraina, S., Genovesio, A., Marconi, B., Squatrito, S., Molinari, M., Lacquaniti, F., Caminiti, R., 2001. Eye–hand coordination during reaching. II. An analysis of the relationships between visuomanual signals in parietal cortex and parieto-frontal association projections. *Cereb. Cortex* 11, 528–544.
- Battaglini, P.P., Muzur, A., Galletti, C., Skrap, M., Brovelli, A., Fattori, P., 2002. Effects of lesions to area V6A in monkeys. *Exp. Brain Res.* 144, 419–422.
- Bernier, P.M., Grafton, S.T., 2010. Human posterior parietal cortex flexibly determines reference frames for reaching based on sensory context. *Neuron* 68, 776–788.
- Beurze, S.M., de Lange, F.P., Toni, I., Medendorp, W.P., 2007. Integration of target and effector information in the human brain during reach planning. *J. Neurophysiol.* 97, 188–199.
- Bisley, J.W., Goldberg, M.E., 2010. Attention, intention, and priority in the parietal lobe. *Annu. Rev. Neurosci.* 33, 1–21.
- Biswal, B., Yetkin, F.Z., Haughton, V.M., Hyde, J.S., 1995. Functional connectivity in the motor cortex of resting human brain using echo-planar MRI. *Magn. Reson. Med.* 34, 537–541.
- Brodman, K., 1909. *The Principles of Comparative Localization of the Cerebral Cortex Based on Cytoarchitectonics*. Johann Ambrosius Barth, Leipzig.
- Brodman, K., 2006. Brodman's localization of the cerebral cortex: the principles of comparative localization in the cerebral cortex based on cytoarchitectonics. In: Gary, L. (Ed.), Springer, New York.
- Buckner, R.L., Andrews-Hanna, J.R., Schacter, D.L., 2008. The brain's default network: anatomy, function, and relevance to disease. *Ann. N. Y. Acad. Sci.* 1124, 1–38.
- Buckwalter, J.A., Parvizi, J., Morecraft, R.J., van Hoesen, G.W., 2008. Thalamic projections to the posteromedial cortex in the macaque. *J. Comp. Neurol.* 507, 1709–1733.
- Canavero, S., Massa-Micon, B., Cauda, F., Montanaro, E., 2009. Bifocal extradural cortical stimulation-induced recovery of consciousness in the permanent post-traumatic vegetative state. *J. Neurol.* 256, 834–836.
- Cauda, F., Gemini, G., D'Agata, F., Sacco, K., Duca, S., Bagshaw, A.P., Cavanna, A.E., 2010. Functional connectivity of the posteromedial cortex. *PLoS ONE* 5.
- Cavada, C., Goldman-Raiuc, P.S., 1989. Posterior parietal cortex in rhesus monkey: I. Parcellation of areas based on distinctive limbic and sensory corticocortical connections. *J. Comp. Neurol.* 287, 393–421.
- Cavanna, A.E., Trimble, M.R., 2006. The precuneus: a review of its functional anatomy and behavioural correlates. *Brain* 129, 564–583.
- Cavina-Pratesi, C., Monaco, S., Fattori, P., Galletti, C., McAdam, T.D., Quinlan, D.J., Goodale, M.A., Culham, J.C., 2010. Functional magnetic resonance imaging reveals the neural substrates of arm transport and grip formation in reach-to-grasp actions in humans. *J. Neurosci.* 30, 10306–10323.
- Ciavarrò, M., Ambrosini, E., Tosoni, A., Committeri, G., Fattori, P., Galletti, C., 2013. rTMS of medial parieto-occipital cortex interferes with attentional reorienting during attention and reaching tasks. *J. Cogn. Neurosci.* 25, 1453–1462.
- Cisek, P., Crammond, D.J., Kalaska, J.F., 2003. Neural activity in primary motor and dorsal premotor cortex in reaching tasks with the contralateral versus ipsilateral arm. *J. Neurophysiol.* 89, 922–942.
- Cohen, A.L., Fair, D.A., Dosenbach, N.U., Miezin, F.M., Dierker, D., Van Essen, D.C., Schlaggar, B.L., Petersen, S.E., 2008. Defining functional areas in individual human brains using resting functional connectivity MRI. *NeuroImage* 41, 45–57.
- Colby, C.L., Gattass, R., Olson, C.R., Gross, C.G., 1988. Topographical organization of cortical afferents to extrastriate visual area PO in the macaque: a dual tracer study. *J. Comp. Neurol.* 269, 392–413.
- Connolly, J.D., Andersen, R.A., Goodale, M.A., 2003. fMRI evidence for a 'parietal reach region' in the human brain. *Exp. Brain Res.* 153, 140–145.
- Corbetta, M., Shulman, G.L., 2002. Control of goal-directed and stimulus-driven attention in the brain. *Nat. Rev. Neurosci.* 3, 201–215.
- Culham, J.C., Valyear, K.F., 2006. Human parietal cortex in action. *Curr. Opin. Neurobiol.* 16, 205–212.
- Culham, J.C., Cavina-Pratesi, C., Singhal, A., 2006. The role of parietal cortex in visuomotor control: what have we learned from neuroimaging? *Neuropsychologia* 44, 2668–2684.
- Davis, M.H., Johnsrude, I.S., 2003. Hierarchical processing in spoken language comprehension. *J. Neurosci.* 23, 3423–3431.
- Deco, G., Corbetta, M., 2011. The dynamical balance of the brain at rest. *Neuroscientist* 17, 107–123.
- Deco, G., Jirsa, V.K., McIntosh, A.R., 2011. Emerging concepts for the dynamical organization of resting-state activity in the brain. *Nat. Rev. Neurosci.* 12, 43–56.
- Dorfl, D., Werner, A., Schaefer, M., von Kummer, R., Karl, A., 2009. Distinct brain networks in recognition memory share a defined region in the precuneus. *Eur. J. Neurosci.* 30, 1947–1959.
- Dum, R.P., Strick, P.L., 2002. Motor areas in the frontal lobe of the primate. *Physiol. Behav.* 77, 677–682.
- Duvernoy, Henri, M., 2012. *The human brain: surface, three-dimensional sectional anatomy with MRI, and blood supply*. Springer Science & Business Media.
- Economo, C., Koskinas, G.N., 1925. *The Cytoarchitectonics of the Cerebral Cortex of the Human Adult*. Julius Springer, Vienna-Berlin.
- Evans, A.C., Collins, D.L., Mills, S.R., Brown, E.D., Kelly, R.L., Peters, T.M., 1993. 3D statistical neuroanatomical models from 305 MRI volumes. *Proceedings of the IEEE—Nuclear Science Symposium and Medical Imaging Conference*, pp. 1813–1817.
- Farber, N.E., Harkin, C.P., Niedfeldt, J., Hudetz, A.G., Kampine, J.P., Schmeling, W.T., 1997. Region-specific and agent-specific dilation of intracerebral microvessels by volatile anesthetics in rat brain slices. *Anesthesiology* 87, 1191–1198.
- Fattori, P., Pitzalis, S., Galletti, C., 2009a. The cortical visual area V6 in macaque and human brains. *J. Physiol. Paris* 103, 88–97.
- Fattori, P., Gamberini, M., Kutz, D.F., Galletti, C., 2001. 'Arm-reaching' neurons in the parietal area V6A of the macaque monkey. *Eur. J. Neurosci.* 13, 2309–2313.
- Fattori, P., Kutz, D.F., Breveglieri, R., Marzocchi, N., Galletti, C., 2005. Spatial tuning of reaching activity in the medial parieto-occipital cortex (area V6A) of macaque monkey. *Eur. J. Neurosci.* 22, 956–972.
- Fattori, P., Breveglieri, R., Raos, V., Bosco, A., Galletti, C., 2012. Vision for action in the macaque medial posterior parietal cortex. *J. Neurosci.* 32, 3221–3234.
- Fattori, P., Breveglieri, R., Marzocchi, N., Filippini, D., Bosco, A., Galletti, C., 2009b. Hand orientation during reach-to-grasp movements modulates neuronal activity in the medial posterior parietal area V6A. *J. Neurosci.* 29, 1928–1936.
- Fattori, P., Raos, V., Breveglieri, R., Bosco, A., Marzocchi, N., Galletti, C., 2010. The dorsomedial pathway is not just for reaching: grasping neurons in the medial parieto-occipital cortex of the macaque monkey. *J. Neurosci.* 30, 342–349.
- Felleman, D.J., Burkhalter, A., Van Essen, D.C., 1997. Cortical connections of areas V3 and VP of macaque monkey extrastriate visual cortex. *J. Comp. Neurol.* 379, 21–47.
- Ferraina, S., Battaglia-Mayer, A., Genovesio, A., Marconi, B., Onorati, P., Caminiti, R., 2001. Early coding of visuomanual coordination during reaching in parietal area PEc. *J. Neurophysiol.* 85, 462–467.
- Filimon, F., 2010. Human cortical control of hand movements: parietofrontal networks for reaching, grasping, and pointing. *Neuroscientist* 16, 388–407.
- Filimon, F., Nelson, J.D., Huang, R.S., Sereno, M.I., 2009. Multiple parietal reach regions in humans: cortical representations for visual and proprioceptive feedback during online reaching. *J. Neurosci.* 29, 2961–2971.
- Fiset, P., Paus, T., Daloze, T., Plourde, G., Meuret, P., Bonhomme, V., Hajj-Ali, N., Backman, S.B., Evans, A.C., 1999. Brain mechanisms of propofol-induced loss of consciousness in humans: a positron emission tomographic study. *J. Neurosci.* 19, 5506–5513.

- Fox, M.D., Raichle, M.E., 2007. Spontaneous fluctuations in brain activity observed with functional magnetic resonance imaging. *Nat. Rev. Neurosci.* 8, 700–711.
- Galletti, C., Fattori, P., Gamberini, M., Kutz, D.F., 1999. The cortical visual area V6: brain location and visual topography. *Eur. J. Neurosci.* 11, 3922–3936.
- Galletti, C., Fattori, P., Battaglini, P.P., Shipp, S., Zeki, S., 1996. Functional demarcation of a border between areas V6 and V6A in the superior parietal gyrus of the macaque monkey. *Eur. J. Neurosci.* 8, 30–52.
- Galletti, C., Gamberini, M., Kutz, D.F., Baldinotti, I., Fattori, P., 2005. The relationship between V6 and PO in macaque extrastriate cortex. *Eur. J. Neurosci.* 21, 959–970.
- Galletti, C., Gamberini, M., Kutz, D.F., Fattori, P., Luppino, G., Matelli, M., 2001. The cortical connections of area V6: an occipito-parietal network processing visual information. *Eur. J. Neurosci.* 13, 1572–1588.
- Gallivan, J.P., Cavina-Pratesi, C., Culham, J.C., 2009. Is that within reach? fMRI reveals that the human superior parieto-occipital cortex encodes objects reachable by the hand. *J. Neurosci.* 29, 4381–4391.
- Gallivan, J.P., Johnsrude, I.S., Randall Flanagan, J., 2015. Planning ahead: object-directed sequential actions decoded from human frontoparietal and occipitotemporal networks. *Cereb. Cortex.*
- Gallivan, J.P., McLean, D.A., Smith, F.W., Culham, J.C., 2011a. Decoding effector-dependent and effector-independent movement intentions from human parieto-frontal brain activity. *J. Neurosci.* 31, 17149–17168.
- Gallivan, J.P., McLean, D.A., Flanagan, J.R., Culham, J.C., 2013. Where one hand meets the other: limb-specific and action-dependent movement plans decoded from preparatory signals in single human frontoparietal brain areas. *J. Neurosci.* 33, 1991–2008.
- Gallivan, J.P., McLean, D.A., Valyear, K.F., Pettepiece, C.E., Culham, J.C., 2011b. Decoding action intentions from preparatory brain activity in human parieto-frontal networks. *J. Neurosci.* 31, 9599–9610.
- Gamberini, M., Galletti, C., Bosco, A., Breveglieri, R., Fattori, P., 2011. Is the medial posterior parietal area V6A a single functional area? *J. Neurosci.* 31, 5145–5157.
- Gamberini, M., Passarelli, L., Fattori, P., Zucchelli, M., Bakola, S., Luppino, G., Galletti, C., 2009. Cortical connections of the visuomotor parietooccipital area V6Ad of the macaque monkey. *J. Comp. Neurol.* 513, 622–642.
- Goodale, M.A., Milner, A.D., 1992. Separate visual pathways for perception and action. *Trends Neurosci.* 15, 20–25.
- Hickok, G., Poeppel, D., 2000. Towards a functional neuroanatomy of speech perception. *Trends Cogn. Sci.* 4, 131–138.
- Hickok, G., Poeppel, D., 2007. The cortical organization of speech processing. *Nat. Rev. Neurosci.* 8, 393–402.
- Hill, J., Inder, T., Neil, J., Dierker, D., Harwell, J., Van Essen, D., 2010. Similar patterns of cortical expansion during human development and evolution. *Proc. Natl. Acad. Sci. U. S. A.* 107, 13135–13140.
- Hutchison, R.M., Everling, S., 2012. Monkey in the middle: why non-human primates are needed to bridge the gap in resting-state investigations. *Front. Neuroanat.* 6, 29.
- Hutchison, R.M., Everling, S., 2013. Broad intrinsic functional connectivity boundaries of the macaque prefrontal cortex. *NeuroImage* 88C, 202–211.
- Hutchison, R.M., Mirsattari, S.M., Jones, C.K., Gati, J.S., Leung, L.S., 2010. Functional networks in the anesthetized rat brain revealed by independent component analysis of resting-state fMRI. *J. Neurophysiol.* 103, 3398–3406.
- Hutchison, R.M., Womelsdorf, T., Gati, J.S., Everling, S., Menon, R.S., 2012a. Resting-state networks show dynamic functional connectivity in awake humans and anesthetized macaques. *Hum. Brain Mapp.* 34, 2154–2177.
- Hutchison, R.M., Hutchison, M., Manning, K.Y., Menon, R.S., Everling, S., 2014a. Isoflurane induces dose-dependent alterations in the cortical connectivity profiles and dynamic properties of the brain's functional architecture. *Hum. Brain Mapp.* 35, 5754–5775.
- Hutchison, R.M., Culham, J.C., Everling, S., Flanagan, J.R., Gallivan, J.P., 2014b. Distinct and distributed functional connectivity patterns across cortex reflect the domain-specific constraints of object, face, scene, body, and tool category-selective modules in the ventral visual pathway. *NeuroImage* 96, 216–236.
- Hutchison, R.M., Leung, L.S., Mirsattari, S.M., Gati, J.S., Menon, R.S., Everling, S., 2011. Resting-state networks in the macaque at 7 T. *NeuroImage* 56, 1546–1555.
- Hutchison, R.M., Womelsdorf, T., Gati, J.S., Leung, L.S., Menon, R.S., Everling, S., 2012b. Resting-state connectivity identifies distinct functional networks in macaque cingulate cortex. *Cereb. Cortex* 22, 1294–1308.
- Hutchison, R.M., Gallivan, J.P., Culham, J.C., Gati, J.S., Menon, R.S., Everling, S., 2012c. Functional connectivity of the frontal eye fields in humans and macaque monkeys investigated with resting-state fMRI. *J. Neurophysiol.* 107, 2463–2474.
- Hutchison, R.M., Womelsdorf, T., Allen, E.A., Bandettini, P.A., Calhoun, V.D., Corbetta, M., Penna, S.D., Duyn, J., Glover, G., Gonzalez-Castillo, J., Handwerker, D.A., Keilholz, S., Kiviniemi, V., Leopold, D.A., de Pasquale, F., Sporns, O., Walter, M., Chang, C., 2013. Dynamic functional connectivity: promises, issues, and interpretations. *NeuroImage* 80, 360–378.
- Hutzler, F., 2013. Reverse inference is not a fallacy per se: cognitive processes can be inferred from functional imaging data. *NeuroImage* 84, 1061–1069.
- Hwang, E.J., Hauschild, M., Wilke, M., Andersen, R.A., 2012. Inactivation of the parietal reach region causes optic ataxia, impairing reaches but not saccades. *Neuron* 76, 1021–1029.
- Johansen-Berg, H., Behrens, T.E., Robson, M.D., Drobnyak, I., Rushworth, M.F., Brady, J.M., Smith, S.M., Higham, D.J., Matthews, P.M., 2004. Changes in connectivity profiles define functionally distinct regions in human medial frontal cortex. *Proc. Natl. Acad. Sci. U. S. A.* 101, 13335–13340.
- Kalaska, J.F., Scott, S.H., Cisek, P., Sergio, L.E., 1997. Cortical control of reaching movements. *Curr. Opin. Neurobiol.* 7, 849–859.
- Karnath, H.O., Perenin, M.T., 2005. Cortical control of visually guided reaching: evidence from patients with optic ataxia. *Cereb. Cortex* 15, 1561–1569.
- Kobayashi, Y., Amaral, D.G., 2003. Macaque monkey retrosplenial cortex: II. Cortical afferents. *J. Comp. Neurol.* 466, 48–79.
- Kobayashi, Y., Amaral, D.G., 2007. Macaque monkey retrosplenial cortex: III. Cortical efferents. *J. Comp. Neurol.* 502, 810–833.
- Kravitz, D.J., Saleem, K.S., Baker, C.I., Mishkin, M., 2011. A new neural framework for visuospatial processing. *Nat. Rev. Neurosci.* 12, 217–230.
- Kravitz, D.J., Saleem, K.S., Baker, C.I., Ungerleider, L.G., Mishkin, M., 2013. The ventral visual pathway: an expanded neural framework for the processing of object quality. *Trends Cogn. Sci.* 17, 26–49.
- Leech, R., Braga, R., Sharp, D.J., 2012. Echoes of the brain within the posterior cingulate cortex. *J. Neurosci.* 32, 215–222.
- Leichnetz, G.R., 2001. Connections of the medial posterior parietal cortex (area 7m) in the monkey. *Anat. Rec.* 263, 215–236.
- Lewis, J.W., Van Essen, D.C., 2000a. Mapping of architectonic subdivisions in the macaque monkey, with emphasis on parieto-occipital cortex. *J. Comp. Neurol.* 428, 79–111.
- Lewis, J.W., Van Essen, D.C., 2000b. Corticocortical connections of visual, sensorimotor, and multimodal processing areas in the parietal lobe of the macaque monkey. *J. Comp. Neurol.* 428, 112–137.
- Lundstrom, B.N., Ingvar, M., Petersson, K.M., 2005. The role of precuneus and left inferior frontal cortex during source memory episodic retrieval. *NeuroImage* 27, 824–834.
- Lundstrom, B.N., Petersson, K.M., Andersson, J., Johansson, M., Fransson, P., Ingvar, M., 2003. Isolating the retrieval of imagined pictures during episodic memory: activation of the left precuneus and left prefrontal cortex. *NeuroImage* 20, 1934–1943.
- Luppino, G., Ben Hamed, S., Gamberini, M., Matelli, M., Galletti, C., 2005. Occipital (V6) and parietal (V6A) areas in the anterior wall of the parieto-occipital sulcus of the macaque: a cytoarchitectonic study. *Eur. J. Neurosci.* 21, 3056–3076.
- Mantini, D., Corbetta, M., Romani, G.L., Orban, G.A., Vanduffel, W., 2013. Evolutionarily novel functional networks in the human brain? *J. Neurosci.* 33, 3259–3275.
- Maquet, P., Degueldre, C., Delfiore, G., Aerts, J., Peters, J.M., Luxen, A., Franck, G., 1997. Functional neuroanatomy of human slow wave sleep. *J. Neurosci.* 17, 2807–2812.
- Margulies, D.S., Vincent, J.L., Kelly, C., Lohmann, G., Uddin, L.Q., Biswal, B.B., Villringer, A., Castellanos, F.X., Milham, M.P., Petrides, M., 2009. Precuneus shares intrinsic functional architecture in humans and monkeys. *Proc. Natl. Acad. Sci. U. S. A.* 106, 20069–20074.
- Mars, R.B., Jbabdi, S., Sallet, J., O'Reilly, J.X., Croxson, P.L., Olivier, E., Noonan, M.P., Bergmann, C., Mitchell, A.S., Baxter, M.G., Behrens, T.E., Johansen-Berg, H., Tomassini, V., Miller, K.L., Rushworth, M.F., 2011. Diffusion-weighted imaging tractography-based parcellation of the human parietal cortex and comparison with human and macaque resting-state functional connectivity. *J. Neurosci.* 31, 4087–4100.
- Masamoto, K., Kanno, I., 2012. Anesthesia and the quantitative evaluation of neurovascular coupling. *J. Cereb. Blood Flow Metab.* 32, 1233–1247.
- Michener, C.D., Sokal, R.R., 1957. A quantitative approach to a problem of classification. *Evolution* 11, 490–499.
- Monaco, S., Cavina-Pratesi, C., Sedda, A., Fattori, P., Galletti, C., Culham, J.C., 2011. Functional magnetic resonance adaptation reveals the involvement of the dorsomedial stream in hand orientation for grasping. *J. Neurophysiol.* 105, 2248–2263.
- Moore, T., Armstrong, K.M., Fallah, M., 2003. Visuomotor origins of covert spatial attention. *Neuron* 40, 671–683.
- Morecraft, R.J., Cipolloni, P.B., Stilwell-Morecraft, K.S., Gedney, M.T., Pandya, D.N., 2004. Cytoarchitecture and cortical connections of the posterior cingulate and adjacent somatosensory fields in the rhesus monkey. *J. Comp. Neurol.* 469, 37–69.
- Morris, R., Petrides, M., Pandya, D.N., 1999. Architecture and connections of retrosplenial area 30 in the rhesus monkey (*Macaca mulatta*). *Eur. J. Neurosci.* 11, 2506–2518.
- Murphy, K., Birn, R.M., Handwerker, D.A., Jones, T.B., Bandettini, P.A., 2009. The impact of global signal regression on resting state correlations: are anti-correlated networks introduced? *NeuroImage* 44, 893–905.
- Neubert, F.X., Mars, R.B., Thomas, A.G., Sallet, J., Rushworth, M.F., 2014. Comparison of human ventral frontal cortex areas for cognitive control and language with areas in monkey frontal cortex. *Neuron* 81, 700–713.
- Pandya, D.N., Seltzer, B., 1982. Intrinsic connections and architectonics of posterior parietal cortex in the rhesus monkey. *J. Comp. Neurol.* 204, 196–210.
- Parvizi, J., Van Hoesen, G.W., Buckwalter, J., Damasio, A., 2006. Neural connections of the posteromedial cortex in the macaque. *Proc. Natl. Acad. Sci. U. S. A.* 103, 1563–1568.
- Passarelli, L., Rosa, M.G., Gamberini, M., Bakola, S., Burman, K.J., Fattori, P., Galletti, C., 2011. Cortical connections of area V6Av in the macaque: a visual-input node to the eye/hand coordination system. *J. Neurosci.* 31, 1790–1801.
- Perenin, M.T., Vighetto, A., 1988. Optic ataxia: a specific disruption in visuomotor mechanisms. I. Different aspects of the deficit in reaching for objects. *Brain* 111, 643–674.
- Pitzalis, S., Sereno, M.I., Committeri, G., Fattori, P., Galati, G., Patria, F., Galletti, C., 2010. Human v6: the medial motion area. *Cereb. Cortex* 20, 411–424.
- Pitzalis, S., Sereno, M.I., Committeri, G., Fattori, P., Galati, G., Tsoni, A., Galletti, C., 2013a. The human homologue of macaque area V6A. *NeuroImage* 82, 517–530.
- Pitzalis, S., Galletti, C., Huang, R.S., Patria, F., Committeri, G., Galati, G., Fattori, P., Sereno, M.I., 2006. Wide-field retinotopy defines human cortical visual area v6. *J. Neurosci.* 26, 7962–7973.
- Pitzalis, S., Sdoia, S., Bultrini, A., Committeri, G., Di Russo, F., Fattori, P., Galletti, C., Galati, G., 2013b. Selectivity to translational egomotion in human brain motion areas. *PLoS ONE* 8, e60241.
- Poldrack, R.A., 2006. Can cognitive processes be inferred from neuroimaging data? *Trends Cogn. Sci.* 10, 59–63.
- Poldrack, R.A., 2011. Inferring mental states from neuroimaging data: from reverse inference to large-scale decoding. *Neuron* 72, 692–697.
- Power, J.D., Cohen, A.L., Nelson, S.M., Wig, G.S., Barnes, K.A., Church, J.A., Vogel, A.C., Laumann, T.O., Miezin, F.M., Schlaggar, B.L., Petersen, S.E., 2011. Functional network organization of the human brain. *Neuron* 72, 665–678.

- Prado, J., Clavagnier, S., Otzenberger, H., Scheiber, C., Kennedy, H., Perenin, M.T., 2005. Two cortical systems for reaching in central and peripheral vision. *Neuron* 48, 849–858.
- Sallet, J., Mars, R.B., Noonan, M.P., Neubert, F.X., Jbabdi, S., O'Reilly, J.X., Filippini, N., Thomas, A.G., Rushworth, M.F., 2013. The organization of dorsal frontal cortex in humans and macaques. *J. Neurosci.* 33, 12255–12274.
- Scheperjans, F., Hermann, K., Eickhoff, S.B., Amunts, K., Schleicher, A., Zilles, K., 2008a. Observer-independent cytoarchitectonic mapping of the human superior parietal cortex. *Cereb. Cortex* 18, 846–867.
- Scheperjans, F., Eickhoff, S.B., Homke, L., Mohlberg, H., Hermann, K., Amunts, K., Zilles, K., 2008b. Probabilistic maps, morphometry, and variability of cytoarchitectonic areas in the human superior parietal cortex. *Cereb. Cortex* 18, 2141–2157.
- Schilbach, L., Eickhoff, S.B., Rotarska-Jagiela, A., Fink, G.R., Vogeley, K., 2008. Minds at rest? Social cognition as the default mode of cognizing and its putative relationship to the “default system” of the brain. *Conscious. Cogn.* 17, 457–467.
- Schilbach, L., Bzdok, D., Timmermans, B., Fox, P.T., Laird, A.R., Vogeley, K., Eickhoff, S.B., 2012. Introspective minds: using ALE meta-analyses to study commonalities in the neural correlates of emotional processing, social & unconstrained cognition. *PLoS ONE* 7, e30920.
- Scholvinck, M.L., Maier, A., Ye, F.Q., Duyn, J.H., Leopold, D.A., 2010. Neural basis of global resting-state fMRI activity. *Proc. Natl. Acad. Sci. U. S. A.* 107, 10238–10243.
- Serrien, D.J., Ivry, R.B., Swinnen, S.P., 2006. Dynamics of hemispheric specialization and integration in the context of motor control. *Nat. Rev. Neurosci.* 7, 160–166.
- Shen, K., Bezgin, G., Hutchison, R.M., Gati, J.S., Menon, R.S., Everling, S., McIntosh, A.R., 2012. Information processing architecture of functionally defined clusters in the macaque cortex. *J. Neurosci.* 32, 17465–17476.
- Silver, M.A., Kastner, S., 2009. Topographic maps in human frontal and parietal cortex. *Trends Cogn. Sci.* 13, 488–495.
- Silver, M.A., Ress, D., Heeger, D.J., 2005. Topographic maps of visual spatial attention in human parietal cortex. *J. Neurophysiol.* 94, 1358–1371.
- Smith, E.G., 1907. A new topographical survey of the human cerebral cortex, being an account of the distribution of the anatomically distinct cortical areas and their relationship to cerebral sulci. *J. Anat. Physiol.* 41, 237–254.
- Smith, S.M., Jenkinson, M., Woolrich, M.W., Beckmann, C.F., Behrens, T.E., Johansen-Berg, H., Bannister, P.R., De Luca, M., Drobnjak, I., Flitney, D.E., Niazy, R.K., Saunders, J., Vickers, J., Zhang, Y., De Stefano, N., Brady, J.M., Matthews, P.M., 2004. Advances in functional and structural MR image analysis and implementation as FSL. *NeuroImage* 23 (Suppl. 1), S208–S219.
- Tosoni, A., Pitzalis, S., Committeri, G., Fattori, P., Galletti, C., Galati, G., 2014. Resting-state connectivity and functional specialization in human medial parieto-occipital cortex. *Brain Struct. Funct.*
- Tzourio-Mazoyer, N., Landeau, B., Papathanassiou, D., Crivello, F., Etard, O., Delcroix, N., Mazoyer, B., Joliot, M., 2002. Automated anatomical labeling of activations in SPM using a macroscopic anatomical parcellation of the MNI MRI single-subject brain. *NeuroImage* 15, 273–289.
- Ungerleider, L.G., Mishkin, M., 1982. Two cortical visual systems. In: Ingle, D.J., Goodale, M.A., Mansfield, R.J.W. (Eds.), *Analysis of Visual Behavior*. MIT Press, Cambridge, MA, pp. 549–586.
- Van Essen, D.C., 2004. Surface-based approaches to spatial localization and registration in primate cerebral cortex. *NeuroImage* 23 (Suppl. 1), S97–S107.
- Van Essen, D.C., 2005. A Population-Average, Landmark- and Surface-based (PALS) atlas of human cerebral cortex. *NeuroImage* 28, 635–662.
- Van Essen, D.C., Drury, H.A., Dickson, J., Harwell, J., Hanlon, D., Anderson, C.H., 2001. An integrated software suite for surface-based analyses of cerebral cortex. *J. Am. Med. Inform. Assoc.* 8, 443–459.
- Vesia, M., Prime, S.L., Yan, X., Sergio, L.E., Crawford, J.D., 2010. Specificity of human parietal saccade and reach regions during transcranial magnetic stimulation. *J. Neurosci.* 30, 13053–13065.
- Vincent, J.L., Patel, G.H., Fox, M.D., Snyder, A.Z., Baker, J.T., Van Essen, D.C., Zempel, J.M., Snyder, L.H., Corbetta, M., Raichle, M.E., 2007. Intrinsic functional architecture in the anaesthetized monkey brain. *Nature* 447, 83–86.
- Vogt, B.A., 2009. Architecture, neurocytology and comparative organization of monkey and human cingulate cortices. *Cingulate Neurobiol. Dis.* 65–93.
- Vogt, O., 1911. The myeloarchitectonics of parietal isocortex. *J. Psychol. Neurol.* 18, 379–396.
- Von Bonin, G., Bailey, P., 1947. The neocortex of *Macaca mulatta*. *Illinois Monogr. Med. Sci.* 5 (4).
- Wenderoth, N., Debaere, F., Snaert, S., Swinnen, S.P., 2005. The role of anterior cingulate cortex and precuneus in the coordination of motor behaviour. *Eur. J. Neurosci.* 22, 235–246.
- Woolrich, M.W., Jbabdi, S., Patenaude, B., Chappell, M., Makni, S., Behrens, T., Beckmann, C., Jenkinson, M., Smith, S.M., 2009. Bayesian analysis of neuroimaging data in FSL. *NeuroImage* 45, S173–S186.
- Yang, Z., Chang, C., Xu, T., Jiang, L., Handwerker, D.A., Castellanos, F.X., Milham, M.P., Bandettini, P.A., Zuo, X.N., 2014. Connectivity trajectory across lifespan differentiates the precuneus from the default network. *NeuroImage* 89, 45–56.
- Yeo, B.T., Krienen, F.M., Sepulcre, J., Sabuncu, M.R., Lashkari, D., Hollinshead, M., Roffman, J.L., Smoller, J.W., Zollei, L., Polimeni, J.R., Fischl, B., Liu, H., Buckner, R.L., 2011. The organization of the human cerebral cortex estimated by intrinsic functional connectivity. *J. Neurophysiol.* 106, 1125–1165.
- Zhang, S., Li, C.S., 2012. Functional connectivity mapping of the human precuneus by resting state fMRI. *NeuroImage* 59, 3548–3562.
- Zhang, Y., Fan, L., Zhang, Y., Wang, J., Zhu, M., Zhang, Y., Yu, C., Jiang, T., 2014. Connectivity-based parcellation of the human posteromedial cortex. *Cereb. Cortex* 24, 719–727.